



1 **A machine learning approach targeting parameter estimation for plant**
2 **functional type coexistence modeling using ELM-FATES (v2.0)**

3 Lingcheng Li¹, Yilin Fang², Zhonghua Zheng³, Mingjie Shi¹, Marcos Longo⁴, Charles D. Koven⁴,
4 Jennifer A. Holm⁴, Rosie A. Fisher⁵, Nate G. McDowell^{1,6}, Jeffrey Chambers⁴, L. Ruby Leung¹

5 1. Atmospheric Sciences and Global Change Division, Pacific Northwest National Laboratory,
6 Richland, WA, USA

7 2. Earth System and Science Division, Pacific Northwest National Laboratory, Richland, WA,
8 USA

9 3. Department of Earth and Environmental Sciences, The University of Manchester, Manchester,
10 UK

11 4. Climate and Ecosystem Sciences Division, Lawrence Berkeley National Laboratory, Berkeley,
12 CA, USA

13 5. CICERO Center for International Climate and Environmental Research, Oslo, Norway

14 6. School of Biological Sciences, Washington State University, PO Box 644236, Pullman, WA,
15 USA

16 Correspondence to: Lingcheng Li (lingcheng.li@pnnl.gov)



17 **Highlight**

- 18 • Machine learning based surrogate models were developed and used to optimize the
19 selection of the trait parameters in ELM-FATES demographic vegetation model
- 20 • Trait parameters selected by the surrogate models significantly improve the modeling of
21 plant functional type coexistence and reduce model errors.
- 22 • This approach represents a repeatable method for identifying parameter values that
23 satisfy fidelity against observations and coexistence between functional types in
24 vegetation demography models.

25



26 **Abstract**

27 Tropical forest dynamics play crucial roles in the global carbon, water, and energy cycles.
28 Dynamic global vegetation models are the primary tools to simulate terrestrial ecosystem
29 dynamics and their response to climate change. However, realistically simulating the dynamics of
30 competition and coexistence of differing plant functional traits within tropical forests remains a
31 significant challenge. This study aims to improve the modeling of plant functional type (PFT)
32 coexistence in the Functionally Assembled Terrestrial Ecosystem Simulator (FATES), a
33 vegetation demography model implemented in the Energy Exascale Earth System Model (E3SM)
34 land model (ELM), ELM-FATES. Specifically, we explore: (1) whether plant trait relationships
35 established from field measurements can constrain ELM-FATES simulations; and (2) whether
36 machine learning based surrogate models can emulate the complex ELM-FATES model and
37 optimize parameter selections to improve PFT coexistence modeling. We conducted ELM-FATES
38 experiments for a tropical forest site near Manaus, Brazil. We first conducted two ensembles of
39 ELM-FATES experiments, without (Exp-1) and with (Exp-2) consideration of observed trait
40 relationships, respectively. Considering the observed trait relationships (Exp-2) slightly improves
41 ELM-FATES simulations of water, energy, and carbon fluxes, but degrades the simulation of PFT
42 coexistence. Using eXtreme Gradient Boosting (XGBoost) based surrogate models trained on Exp-
43 1, we optimize the trait-related parameters in ELM-FATES to enable PFT coexistence and reduce
44 model errors relative to the field observations. We used parameters selected by the surrogate model
45 to conduct another ensemble of ELM-FATES experiments (Exp-3). The probability of
46 experiments yielding PFT coexistence greatly increases from 21% in Exp-1 to 73% in Exp-3.
47 Further filtering those experiments that allow for PFT coexistence to agree within 15% of the
48 observations, Exp-3 still has 33% of experiments left, much higher than the 1.4% in Exp-1. Exp-
49 3 also better reproduces the annual means and seasonal variations of water, energy and carbon
50 fluxes, and the field inventory of above ground biomass. Our study demonstrates the benefits of
51 using machine learning models to improve PFT coexistence modeling in ELM-FATES, with
52 important implications for modeling the response and feedback of ecosystem dynamics to climate
53 change. Our results also suggest that new mechanisms are required for robust simulation of
54 coexisting plants in FATES.

55



56 **Plain Language Summary**

57 Modeling tropical forest dynamics is crucial for understanding global carbon, water, and energy
58 cycles under climate change. Dynamic global vegetation models, the primary tools to simulate
59 terrestrial ecosystem dynamics, face the challenge of realistically modeling the competition and
60 coexistence of different plant functional types (PFT). Our study explores whether (1) using plant
61 trait measurements and (2) developing machine learning based surrogate models to optimize
62 parameter selections can improve plant coexistence modeling. Using ELM-FATES as a testbed,
63 multiple ensembles of numerical experiments are conducted for a tropical forest site. We found
64 there is limited guidance of observed trait relationships for PFT coexistence modeling in ELM-
65 FATES. Trait parameters selected by the surrogate models significantly improve the modeling of
66 PFT coexistence and reduce model errors. We demonstrate the benefits of developing machine
67 learning based surrogate models to improve PFT coexistence modeling in ELM-FATES, with
68 important implications for modeling the response and feedback of ecosystem dynamics to climate
69 change. Our results also suggest that new mechanisms are required for robust simulation of
70 coexisting plants in ELM-FATES.

71



72 **1. Introduction**

73 Tropical ecosystems feature the highest biodiversity on Earth, maintaining more than 75% of all
74 known species (Mora et al., 2011; Mitchard, 2018). The dynamics of tropical forests are closely
75 related to the regional and global carbon, energy and water cycles (Bonan, 2008; Piao et al., 2020).
76 Vegetation is expected to face more water stress from vapor pressure deficit increase and soil
77 moisture reduction with global warming (McDowell et al., 2020). Forest dynamics of tree
78 mortality are accelerating in some tropical regions due to the rising atmospheric water stress
79 (Bauman et al., 2022; Hubau et al., 2020; Zuleta et al., 2017). Tropical forests currently make an
80 approximately neutral contribution to the global carbon cycle as a result of a large land-use source
81 balanced by sinks in recovering and undisturbed forests, but they may become a carbon source in
82 the future under the threat of climate change and human-induced disturbance (Mitchard, 2018;
83 Gatti et al., 2021). Therefore, understanding and modeling tropical forest dynamics and related
84 feedbacks have crucial implications for projecting future changes in the global climate system.

85

86 Dynamic global vegetation models (DGVMs) are the primary tools to simulate terrestrial
87 ecosystem dynamics of plant functional type distribution, ecosystem composition and functioning,
88 and ecosystem response to and recovery from disturbance (e.g., fire and wind damage) (Longo et
89 al., 2019; Fisher et al., 2018; Foley et al., 1996; Sitch et al., 2003; Cao and Woodward, 1998;
90 Berzaghi et al., 2019; McMahon et al., 2011). Conventional DGVMs represent plant communities
91 using an area-averaged representation of plant functional types (PFTs) in each grid cell. Their
92 relatively simple structures have the advantage of high computational efficiency for use in Earth
93 system models (Fisher et al., 2018; Snell et al., 2014). However, these models do not capture many
94 demographic processes. For example, plants of each represented PFT typically have identical



95 properties (e.g., tree size), which limits the capability of modeling ecosystem dynamics and
96 functioning of canopy gap formation, PFT competition, and disturbance reactions (Feeley et al.,
97 2007; Stark et al., 2012; Hurtt et al., 1998; Moorcroft, 2003; Brister et al., 2020). To overcome
98 these limitations, individual-based models, also known as forest gap models, explicitly represent
99 vegetation as individual plants and simulate their birth, growth, and death (Fyllas et al., 2014;
100 Christoffersen et al., 2016; Sato et al., 2007; Jonard et al., 2020; Maréchaux and Chave, 2017).
101 These models incorporate the stochasticity and heterogeneity of the plant light environment
102 mechanistically and thereby can typically represent PFT competitive exclusion, succession, and
103 coexistence. However, explicit simulations of individual plants with stochastic processes suffer a
104 substantial computational penalty and limit applicability over large or global scales (Fisher et al.,
105 2018). To capture sufficient ecosystem dynamics and maintain relatively high computational
106 efficiency, "cohort-based" models have been proposed (Haverd et al., 2013; Medvigy et al., 2009;
107 Ma et al., 2021; Moorcroft et al., 2001; Longo et al., 2019). In a cohort-based approach, individual
108 plants are grouped together as "cohorts" based on their similar properties, including size, age, and
109 PFT (Fisher et al., 2018). Many cohort-based models have been developed and widely used across
110 regional to global scales. Examples of cohort-based models include the Ecosystem Demography
111 model (ED) (Moorcroft et al., 2001), the Functionally Assembled Terrestrial Ecosystem Simulator
112 (FATES) (Fisher et al., 2018, 2015), and the Geophysical Fluid Dynamics Laboratory (GFDL)
113 Land Model 3 with the Perfect Plasticity Approximation (LM3-PPA) (Weng et al., 2015). Among
114 these models, FATES has been widely used in modeling ecosystem dynamics for multiple
115 ecosystems, e.g., tropical (Holm et al., 2020; Koven et al., 2020; Cheng et al., 2021) and mixed-
116 conifer forests (Buotte et al., 2021), and forest disturbance (Huang et al., 2020).

117



118 Despite ongoing applications, robust simulations of competition and coexistence in cohort-based
119 DGVMs remain a major challenge. In niche-based coexistence theory, coexisting species require
120 both convergence in strategy to adapt to the surrounding environment ("environmental filtering")
121 and divergence in strategy to ensure differentiation in resource requirements ("niche partitioning")
122 (Kraft et al., 2008; Adler et al., 2013). These same constraints apply to coexisting PFTs as modeled
123 by DGVMs. Thus, on the one hand, DGVMs need to include mechanisms involving critical niche
124 dimensions (e.g., light, water, and nutrients). For example, the multi-layer canopy structure in
125 FATES provides vertical light resource differentiation. Another essential aspect is to assign
126 reasonable plant functional traits (i.e., the parameters that define a given plant functional type) to
127 satisfy environmental filtering, ensure niche partitioning, and consequently preserve PFT
128 coexistence. Considering the relatively high computational cost of DGVMs and the host land
129 surface models, it is not feasible to directly apply global optimization methods such as Shuffled
130 Complex Evolution (Duan et al., 1992) to calibrate trait-related parameters, because this could be
131 time-consuming and computationally intensive (Rouholahnejad et al., 2012). Therefore, most
132 previous studies use the filtered ensemble approach to select trait-related parameters involving
133 several steps: 1) generate a parameter ensemble based on reference trait ranges or correlations, 2)
134 conduct ensemble model simulations, and 3) filter the parameter ensemble by coexistence and
135 other criteria (e.g., observation constraints). For example, Huang et al. (2020) applied FATES
136 implemented in the Community Land Model (CLM; herein CLM-FATES) with two tropical PFTs
137 to study forest dynamics at tropical sites. They performed 70 one-at-a-time experiments before
138 obtaining one reasonable parameter set. Buottte et al. (2021) used CLM-FATES to simulate forest
139 dynamics of pine and incense cedar over the Sierra Nevada of California, and their two stages of
140 experiments (360 plus 72 runs) only yielded four sets of parameters that met the given criteria. The



141 filtered ensemble approach has low efficiency, which hinders DGVMs' application to modeling
142 ecosystem dynamics under the changing climate. In addition, trait relationships derived from field
143 measurements are often used to infer parameter selections when simulating coexistence. For
144 example, Longo et al. (2020) used multiple trait relationships derived from various datasets to
145 guide parameter selection for different PFTs in the ED-2.2 model simulations. However, whether
146 the observed trait relationships can efficiently improve PFT coexistence simulation in current
147 DGVMs is still unclear.

148

149 Machine learning (ML) has facilitated Earth science studies (Shen, 2018; Nearing et al., 2021; Zhu
150 et al., 2022; Pal et al., 2019; Jung et al., 2019), possibly providing a promising approach to improve
151 PFT coexistence modeling in DGVMs. ML algorithms have been broadly and successfully
152 employed in recent decades. They can be used as standalone models to predict variables of interest
153 or integrated with process-based models to improve simulations from the latter (Xu and Liang,
154 2021; He et al., 2022). Among these applications, ML has shown advantages as a surrogate model
155 for parameter optimization and sensitivity quantification, including its effectiveness and easy
156 application, its ability to implicitly deal with complex nonlinear correlations and high dimensional
157 data, and handle interactions between variables (Sit et al., 2020; Antoniadis et al., 2020; Tsai et al.,
158 2021). One promising approach is to construct ML-based surrogate models using data from initial
159 model simulations to emulate the relationship between inputs (i.e., model parameters) and model
160 outputs (Wang et al., 2014). Then the computationally inexpensive surrogate model can be
161 efficiently used for parameter optimization and sensitivity analysis. For example, Dagon et al.
162 (2020) implemented artificial neural networks to emulate the satellite leaf area constrained version
163 of CLM5 (Lawrence et al., 2019) and estimated optimal parameters to improve the global



164 simulation of gross primary production and latent heat flux. Sawada (2020) developed an ML
165 surrogate model to optimize the land surface model parameters and improve soil moisture and
166 vegetation dynamics simulations. Watson-Parris et al. (2021) built a general tool to efficiently
167 emulate Earth system models for uncertainty quantification and model calibration. Although
168 employing ML based surrogate models to optimize the trait parameters and hence improve the
169 vegetation dynamics modeling in DGVMs is promising, this area of research is still under-explored.

170

171 This study aims to improve PFT coexistence modeling in DGVMs. The cohort-based FATES
172 implemented in the Energy Exascale Earth System Model (E3SM) land model (ELM; Golaz et al.,
173 2019), i.e., ELM-FATES, is taken as our testbed. The ELM land model simulates surface energy
174 fluxes, soil and canopy biophysics, hydrology, and soil biogeochemistry, whereas FATES
175 simulates live vegetation processes, litter dynamics, and fire. We first examine whether trait
176 relationships constructed from field measurements can help improve ELM-FATES simulations.
177 Second, we explore whether ML based surrogate models can help optimize key trait parameters in
178 ELM-FATES to improve the simulation of PFTs coexistence. Our model experiments are
179 conducted for a tropical rainforest site located in Manaus, Brazil. This paper is organized as
180 follows. Section 2 describes ELM-FATES, summarizes the key functional trait-related parameters,
181 introduces the machine learning algorithms, and explains the overall experimental design. Results
182 are presented in Section 3, followed by Discussions and Conclusions in Section 4 and Section 5,
183 respectively.

184



185 **2. Methodology**

186 **2.1 Study site and data**

187 Our study site is located at kilometer 34 (K34) of the ZF2 road, Manaus, Brazil (latitude: -2.6091
188 S; longitude: -60.2093 W). The K34 site is an old-growth primary forest with minimal human
189 disturbances (Holm et al., 2020). The annual precipitation is about 2252 mm, and the mean
190 temperature is about 26.68 °C (<https://ameriflux.lbl.gov/sites/siteinfo/BR-Ma2>). The wet season is
191 from November to May, and the dry season is from June to October (Fang et al., 2017). Hourly
192 meteorological forcing (i.e., precipitation, air temperature, relative humidity, wind speed, surface
193 pressure) at the K34 eddy covariance flux tower from 2002–2005 was obtained from the LBA-
194 ECO CD-32 Flux Tower Network Data Compilation (Restrepo-Coupe et al., 2021). Observational
195 reference datasets obtained from Holm et al. (2020) include gross primary production (GPP),
196 evapotranspiration (ET), sensible heat flux (SH), Bowen ratio (BW, the ratio between sensible heat
197 and latent heat), and inventory data-based aboveground biomass (AGB). The GPP, ET, SH, and
198 BW observations are monthly climatological averages from 2000 to 2008 (Table S1). The AGB at
199 this site is about 303 ± 2.3 Mg/ha. These observational data were used to evaluate the ELM-
200 FATES simulations and constrain the ML surrogate models.

201

202 **2.2 ELM-FATES and parameters**

203 ELM-FATES is used as the testbed. ELM is the land model of E3SM, which is the host land model
204 of FATES (Golaz et al., 2019; Leung et al., 2020; Holm et al., 2020). FATES is a size- and age-
205 structured vegetation model developed from the Community Land Model with ecosystem
206 demography (CLM-ED) (Fisher et al., 2015; Koven et al., 2020). FATES includes two key
207 structural components: ecosystem demography (ED; Moorcroft et al., 2001) and a modified



208 version of perfect plasticity approximation (PPA, Purves et al., 2008). FATES discretizes the
209 simulated landscape into spatially implicit "*patches*" representing different disturbance histories
210 of the ecosystem since the last disturbance. Within each patch, the hypothetical population of
211 plants is grouped into "*cohorts*": a cohort consists of a population density of trees with similar size
212 and the same plant functional type. Cohorts are organized, via the PPA concept, into canopy layers,
213 and compete for light based on their canopy vertical positions (e.g., canopy layer vs. understory
214 layer). The understory layer is formed when the canopy area becomes greater than the total ground
215 area, and some fraction of each cohort is 'demoted' to the understory as a function of its height.
216 The number of patches and cohorts varies depending on processes, including recruitment, growth,
217 mortality, competition, and disturbance. The modified PPA probabilistically splits cohorts into
218 discrete canopy and understory layers based on a function of their height (Strigul et al., 2008;
219 Fisher et al., 2010). A detailed description of the FATES model can be found in its technical note
220 (Zenodo, <https://doi.org/10.5281/zenodo.3517272>).

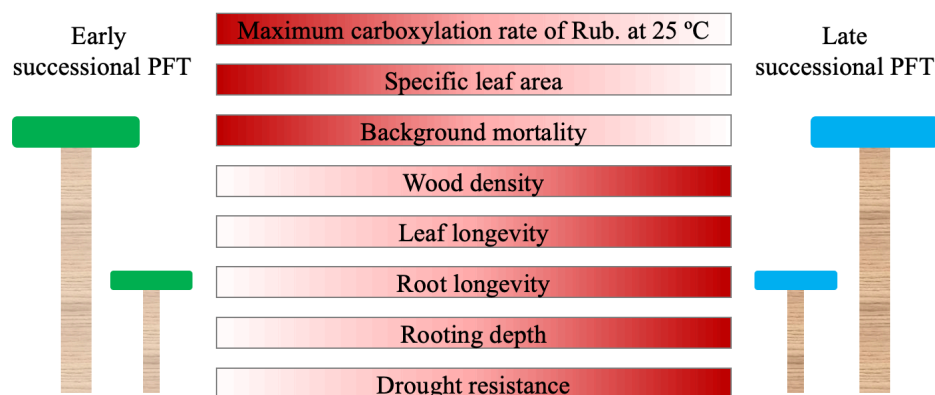
221

222 In this study, we configured two PFTs in ELM-FATES, i.e., early successional and late
223 successional broadleaf evergreen tropical trees, which can represent a primary axis of variability
224 in tropical forests (Huang et al., 2020; Reich, 2014; Díaz et al., 2016). There are tradeoffs between
225 the plant traits of these two PFTs. Compared with the late successional PFT, the early successional
226 PFT is more light-demanding and fast-growing, but with lower woody density, shorter leaf and
227 root lifespans, and higher background mortality. To represent the drought impacts on forest
228 dynamics, the early successional PFT is further assumed to be less drought resistant with shallower
229 rooting depth and hence more easily affected by drought conditions (Oliveira et al., 2021). The



230 corresponding tradeoffs and parameters between these two PFTs are shown in Figure 1 and Table

231 1.



232

233 Figure 1. Schematic representation of tradeoffs between early and late successional PFTs. Dark

234 red denotes a higher parameter value. The tradeoffs of the top five traits are used to constrain the

235 parameter sampling.

236

237 Observational datasets have shown some correlations between plant traits. Therefore, we derived

238 three trait relationships based on the tropical studies of Koven et al. (2020) and Longo et al. (2020).

239 Using the digitized data from Figure 3 in Koven et al. (2020), background mortality M_{bk} (see table

240 1 for parameter definitions) can be empirically computed from V_{cmax} ,

$$241 \quad M_{bk} = 0.0082 \times e^{(0.0153 \times V_{cmax})} \quad (1)$$

242 Based on the equations in Figure S18 of Longo et al. (2020), L_{leaf} and WD can be calculated via

243 SLA ,

$$244 \quad L_{leaf} = 0.0001 \times SLA^{(-2.32)} \quad (2)$$

$$245 \quad WD = -0.583 \times \ln(SLA) - 1.6754 \quad (3)$$



246 These trait relationships are used in parameter generation to test whether considering trait
 247 relationships can help ELM-FATES to model PFT coexistence.

248

249 Table 1 Summary of ELM-FATES parameters for two PFTs

Parameter type	Parameter name	Symbol	Unit	Early PFT	Late PFT	Range
Optimized parameter	Maximum carboxylation rate of Rub. at 25 °C, canopy top	V_{cmax}	$\mu\text{mol CO}_2/\text{m}^2/\text{s}$	$V_{cmax,early} > V_{cmax,late}$		40–105
	Specific leaf area, canopy top	SLA	m^2/gC	$SLA_{early} > SLA_{late}$		0.005–0.04
	Background mortality rate	M_{bk}	1/yr	$M_{bk,early} > M_{bk,late}$		0.005–0.05
	Wood density	WD	g/cm^3	$WD_{early} < WD_{late}$		0.2–1.0
	Leaf longevity	L_{leaf}	year	$L_{leaf,early} < L_{leaf,late}$		0.2–3.0
Fixed parameter	Maximum size of storage C pool, relative to the maximum size of leaf C pool	CR_{szl}	—	same		0.8–1.5
	Root longevity	L_{root}	year	0.9	2.6	—
	Fine rooting distribution profile parameter a	R_a	—	7	7	—
	Fine rooting distribution profile parameter b	R_b	—	2	0.4	—
	BTRAN threshold below which drought mortality begins.	M_{btran}	—	0.4	1.0E-06	—
	Soil water potential at full stomatal closure	$\psi_{closure}$	mm	-113000	-242000	—

250 *Parameter references (Huang et al., 2020; Koven et al., 2020; Longo et al., 2020; Holm et al., 2020; Cheng et al., 2021; Domingues et al.,
 251 2005; Chitra-Tarak et al., 2021; Buotte et al., 2021)

252 * R_a and R_b are parameters that determine the rooting depth and vertical distribution of fine roots.

253 *BTRAN is the plant water stress factor. BTRAN $\in [0,1]$, 0 representing full water stress, 1 representing no water stress.

254

255 2.3 XGboost and SHAP

256 In this study, we built ML-based surrogate models to emulate ELM-FATES simulations. To
 257 represent the nonlinear relationship between ELM-FATES parameters and the model outputs (e.g.,
 258 ET), we used eXtreme Gradient Boosting (XGBoost; Chen and Guestrin, 2016), a decision-tree-
 259 based ensemble machine learning algorithm. The boosting algorithm sequentially trains a set of
 260 weak learners (e.g., decision trees) to the ensemble, with each successive learner correcting the
 261 biases/mistakes of its predecessors. XGBoost is a highly efficient and scalable algorithm built on
 262 the Gradient Boosting framework (Friedman, 2001). For instance, it not only handles complex



263 nonlinear interactions and collinearity between different features (due to the decision tree's nature),
264 but also provides a parallel implementation that effectively solves a range of data science problems.
265 XGBoost has been successfully applied in a variety of fields within Earth and Environmental
266 Sciences, such as urban temperature emulation (Zheng et al., 2021b), wildfire burned area (Wang
267 et al., 2021), and emissions prediction (Wang et al., 2022), flash flood risk assessment (Ma et al.,
268 2021), and aerosol property estimation (Zheng et al., 2021a, c).

269

270 We performed parameter sensitivity analysis to understand which trait parameters are essential for
271 ELM-FATES simulations. A game theoretic approach called SHapley Additive exPlanations
272 (SHAP; Lundberg and Lee, 2017; Lundberg et al., 2018, 2020) was used to interpret the trained
273 XGBoost models and identify the relative importance of features. This approach assumes that
274 features (predictive variables) interact to participate in a game of prediction. The features receive
275 a payout for their contributions as a result of this collaboration. Compared to the intrinsic feature
276 importance methods (for example, feature importance in XGBoost), SHAP uses a unified measure
277 of feature importance to explain both individual samples and the entire dataset (Lundberg and Lee,
278 2017). This novel approach has been used to interpret a digital soil mapping model (Padarian et
279 al., 2020) and identify the critical drivers of wildfires (Wang et al., 2021). Specifically, we
280 performed SHAP analysis for each XGBoost model, and applied the SHAP value as a proxy to
281 quantify the relative importance of different FATES parameters.

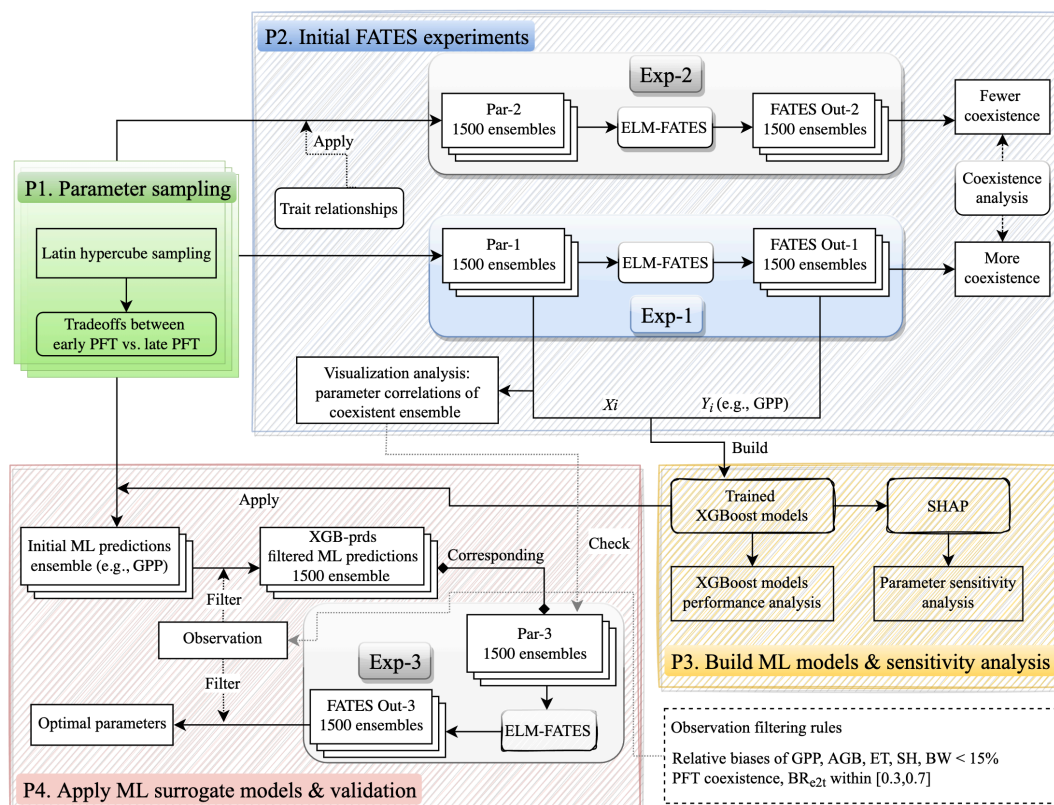
282

283



284 **2.4 Overall experimental design**

285 Our experimental design flowchart is shown in Figure 2. Procedure "P1" in Fig. 2 is used to
 286 generate an ensemble of parameter values for each experiment ensemble, i.e., Exp-1, Exp-2, and
 287 Exp-3. First, a number of initial parameter sets (e.g., 5000 sets) were generated using Latin
 288 Hypercube Sampling (LHS; Mckay et al., 2000). Second, the initial parameter sets were filtered
 289 by the trait tradeoffs between early and late successional PFTs (Figure 1). We repeatedly increased
 290 the number of initial parameter sets in the first step until 1500 parameter sets were obtained in the
 291 second step. Each ELM-FATES experiment starts from bare ground and runs for 350 years to
 292 reach an equilibrium state, by cycling the meteorological forcing during 2002–2005, and the last
 293 four years of the simulations were analyzed.



294



295 Figure 2. Overall flowchart of experimental design and associated analysis.

296 To test whether plant trait relationships established from field measurements can improve the

297 ELM-FATES simulations, two sets of experiment ensembles, i.e., Exp-1 and Exp-2 (procedure

298 "P2" in Figure 2), were conducted using two parameter ensembles (i.e., Par-1 and Par-2). For Par-

299 1, 1500 parameter sets were generated from procedure "P1" based on the entire eleven parameters'

300 space (i.e., $V_{cmax,early}$, $V_{cmax,late}$, SLA_{early} , SLA_{late} , $M_{bk,early}$, $M_{bk,late}$, WD_{early} , WD_{late} ,

301 $L_{leaf,early}$, $L_{leaf,late}$, CR_{s2l}). For Par-2, 1500 parameter sets were generated from procedure "P1"

302 but only based on five parameters' space (i.e., $V_{cmax,early}$, $V_{cmax,late}$, SLA_{early} , SLA_{late} , CR_{s2l}).

303 The other six parameters ($M_{bk,early}$, $M_{bk,late}$, WD_{early} , WD_{late} , $L_{leaf,early}$, $L_{leaf,late}$) in Par-2

304 were calculated based on the traits relationships defined by Equations (1) ~ (3). Therefore,

305 compared to Par-1, the parameters in Par-2 are constrained by the observed trait relationships. The

306 distributions of these two parameter sets are shown in Figure S1. V_{cmax} , SLA , and CR_{s2l} have

307 similar distributions between Par-1 and Par-2. Compared with Par-1, Par-2 has a narrower

308 distribution of M_{bk} but broader distributions of WD and L_{leaf} .

309

310 Exp-1 and Exp-2 each include 1500 350-year ELM-FATES simulations. We averaged the last four

311 years of these simulations for analysis, i.e., outputs: Out-1 and Out-2, respectively. To quantify

312 the PFT coexistence, we computed the biomass ratio between early successional PFT and the total

313 biomass, denoted as BR_{e2t} . For brevity, we denote the ELM-FATES experiments with $BR_{e2t} \in$

314 $[0.1, 0.9]$ as "coexistence", $BR_{e2t} \in [0.0, 0.1]$ as "late", $BR_{e2t} \in (0.9, 1.0]$ as "early". We

315 calculated BR_{e2t} based on Out-1 and Out-2, and then computed the fraction of coexistence

316 experiments in each ensemble. As we will show in section 3.1, considering the observed trait

317 relationships, Exp-2 has a lower fraction of coexistence experiments. Therefore, only Exp-1 was



318 used for further ML-related analysis. We also performed some analysis of Exp-1 to explore
319 whether the parameters of the coexistence experiments have correlations with each other (Section
320 3.2).

321

322 Based on Exp-1, we trained XGBoost models to emulate the ELM-FATES model behavior and
323 analyzed the parameter sensitivity using SHAP (procedure "P3" in Figure 2). Sixteen variables
324 were used as XGBoost model features, including 11 parameters in Par-1 and 5 parameter
325 differences between early and late successional PFTs. The corresponding ELM-FATES annual
326 average outputs were used as XGBoost model targets. Specifically, six models were built, i.e.,
327 XGB_ET, XGB_SH, XGB_BW, XGB_GPP, XGB_AGB, XGB_BR for predicting ET, SH, BW,
328 GPP, AGB, and BR_{e2t} , respectively. Taking BR_{e2t} as an example, the 1500 pairs of sixteen
329 features and the corresponding simulated BR_{e2t} were randomly split into two groups, 90% used
330 for training and the remaining 10% used for testing. In the simulations of Exp-1, the coexistence
331 experiments only account for 20.6% (see Section 3.1 for details). Therefore, 90% of data is used
332 for training to ensure sufficient coexisting samples used in the training process. The choice of
333 hyperparameters in the XGBoost model can significantly impact its performance. In training, we
334 used the Bayesian optimization method to efficiently tune the XGBoost model (Snoek et al., 2012).
335 Additionally, a five-fold cross-validation method was utilized to avoid overfitting in the
336 hyperparameters optimization (Feigl et al., 2021), and the mean squared error was used as the
337 objective function. The root mean squared error (RMSE) and R-squared (R^2) are used to quantify
338 the overall XGBoost model performance for the training and testing data prediction. Furthermore,
339 based on the trained XGBoost models, we applied SHAP to identify feature importance to quantify
340 the parameter sensitivity of ELM-FATES.



341

342 The trained XGBoost models were then used to help select ELM-FATES parameters (procedure
343 "P4" in Figure 2). First, initial parameter sets were generated from procedure "P1" based on the
344 entire eleven parameters' space (Table 1, identical to the parameters' space used for the generation
345 of Par-1). Second, these parameter sets and parameter differences were sent to six XGBoost
346 surrogate models to predict ET, SH, BW, GPP, AGB, and BR_{e2t} . Third, the predictions were
347 further filtered by two criteria: (1) compared to observations, the relative biases of the predicted
348 ET, SH, BW, GPP, and AGB should be less than 15%; (2) the XGBoost model predicted BR_{e2t}
349 should be within [0.3, 0.7]. We repeated these three steps until we obtained 1500 sets of XGBoost
350 model predictions that match the criteria. Finally, we obtained 1500 sets of XGBoost model
351 predictions and their corresponding 1500 sets of parameters (Par-3). We also checked whether the
352 selected Par-3 can match the empirical relationships derived from the empirical analysis in
353 procedure "P2" (see Sections 3.2 and 3.5 for details). Then, the 1500 sets of parameters in Par-3
354 were sent to ELM-FATES to conduct 350-year runs (i.e., Exp-3). The last four years of the
355 simulations were averaged (i.e., Out-3) for further analysis. We then compared Out-3 with
356 observations and analyzed the PFT coexistence to obtain the optimal ELM-FATES parameters.

357

358

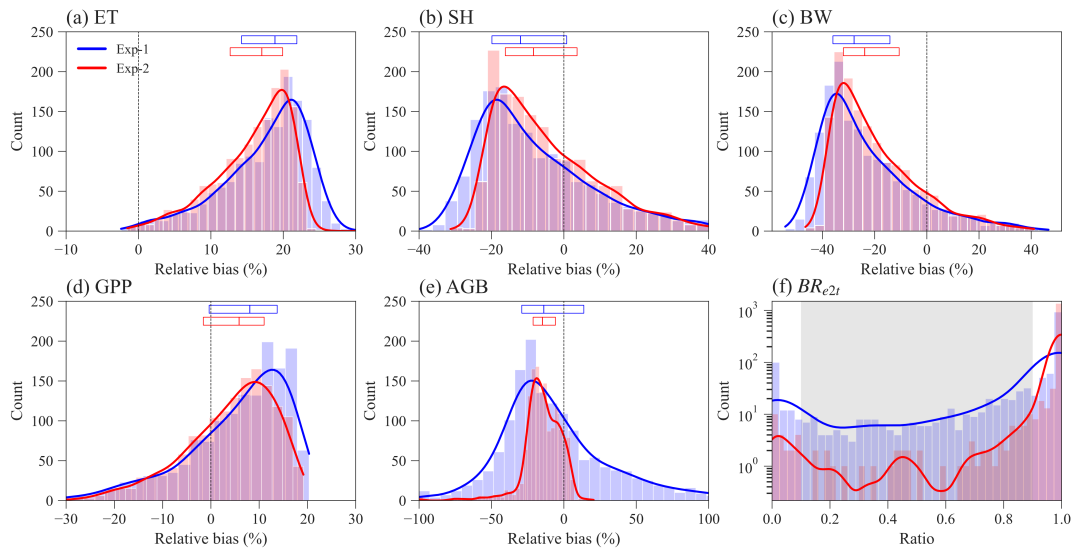


359 **3. Results**

360 **3.1 Comparison between Exp-1 and Exp-2**

361 Constraining the input traits using the observed trait relationships yields slightly better ELM-
362 FATES simulations of water, energy, and carbon variables (Figures 3a~3e). The distributions of
363 the relative biases of ET, SH, BW, and GPP have similar ranges between the two sets of
364 experiments (Figures 3a~3d). Compared with Exp-1, the 50th percentiles of relative biases of ET,
365 SH, BW and GPP for Exp-2 (with constrained traits) are closer to zero, indicating Exp-2 is slightly
366 better than Exp-1. The distribution of simulated AGB for Exp-2 is much narrower than Exp-1
367 (Figure 3e), which could be due to the narrower distribution of M_{bk} (Figure S1).

368 Exp-1 has a much higher fraction of PFT coexisting simulations than Exp-2 (Figure 3f and Table
369 S2). Overall, 70.6 % of experiments in Exp-1, and 94.5% of experiments in EXP-2 have high
370 simulated BR_{e2t} that is greater than 0.9. This indicates that both Par-1 and especially Par-2 favor
371 the early successional PFT. As for the coexisting experiments with $BR_{e2t} \in [0.1, 0.9]$, Exp-1 has
372 about five times more coexisting experiments (20.6%) than Exp-2 (4.1%). Further filtering the
373 coexisting cases by observations (Table S1), only 21 experiments remain in Exp-1, and 6
374 experiments in Exp-2 (Table S2). Even though Exp-2 considered the observed trait relationships,
375 it has fewer coexisting cases within the reasonable observation ranges than Exp-1. Therefore, Exp-
376 2 is not used in our remaining analysis.



377

378 Figure 3. Distribution of ELM-FATES simulations for Exp-1 and Exp-2. The y-axis in (f) is

379 logarithmic. $Relative\ bias = \frac{simulation - observation}{observation} \times 100\ (%)$. In (a)~(e), the top horizontal

380 bars with three vertical lines denote the relative bias at the 25th, 50th, and 75th percentiles,

381 respectively. The grey shaded area in (f) represents the coexistence biomass ratio between 0.1

382 and 0.9.

383 3.2 Parameter analysis of Exp-1

384 We also tested whether simple parameter correlations can be constructed to guide the simulation

385 of PFTs coexistence. No simple parameter correlations can be built to distinguish the coexisting

386 cases from the early and late cases in Exp-1 (Figures 4, S2, and S3). Most parameter (or parameter

387 difference) spaces show large overlaps between early, late, and coexisting cases (Figures S2 and

388 S3). Notably, we empirically built three linear equations based on the boundaries in the parameter

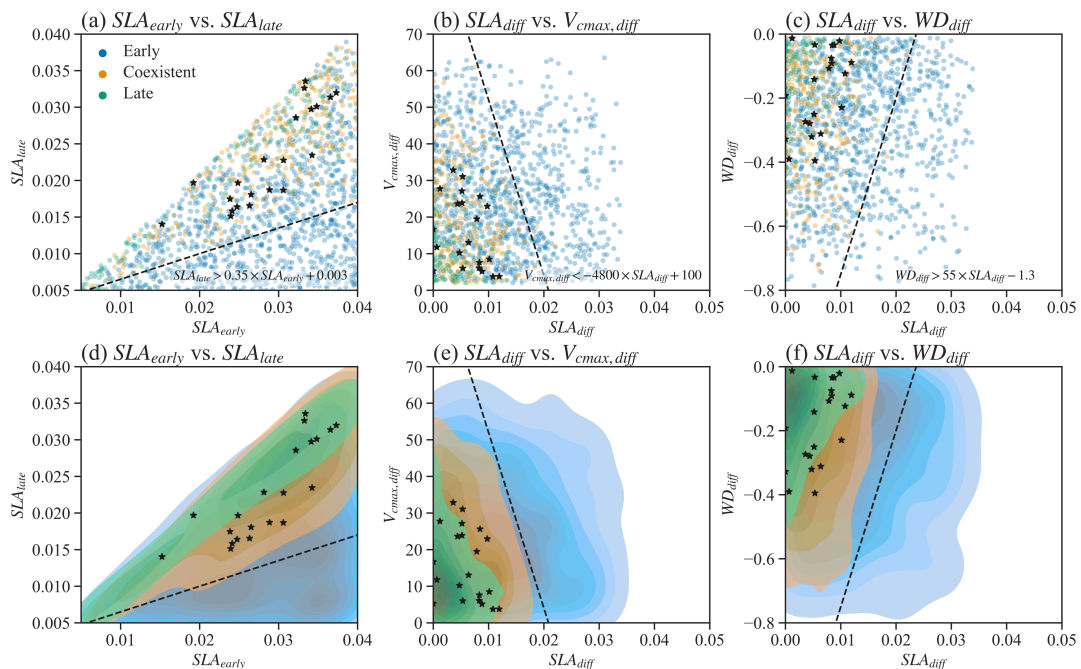
389 spaces for the coexisting cases (Figure 4). Coexisting cases are primarily located in spaces with

390 $SLA_{late} > 0.35 \times SLA_{early} + 0.003$ (Figures 4a and 4d), $V_{cmax,diff} < -4800 \times SLA_{diff} +$

391 100 (Figures 4b and 4e), and $WD_{diff} > 55 \times SLA_{diff} - 1.3$ (Figures 4c and 4f), where



392 $V_{cmax,diff} = V_{cmax,early} - V_{cmax,late}$, and SLA_{diff} and WD_{diff} are defined likewise. Within
 393 these constrained parameter spaces, the percentage of coexisting cases increases from the original
 394 20.6% (i.e., 309 out of 1500) to 32.6% (i.e., 304 out of 932). Therefore, these empirical correlations
 395 could help guide ELM-FATES parameter selection for coexisting PFTs. On the other hand, a
 396 dominant proportion (i.e., 67.4% (1–32.6%)) of experiments are still either early or late cases
 397 within the constrained parameter spaces and cannot robustly predict PFT coexistence. Moreover,
 398 despite further considering the observational constraints (black scatters in Figure 4; Table S2), the
 399 21 experiments (2.3%, 21 out of 932) are still sparsely distributed in the parameters' space of the
 400 coexisting cases, so no simple correlations can be developed based on these simulations. Therefore,
 401 simple empirically built relationships between plant traits provide limited benefit to guiding ELM-
 402 FATES parameter selection for modeling PFTs coexistence while matching the observations. This
 403 finding provides additional motivation for the ML-based approaches.



404

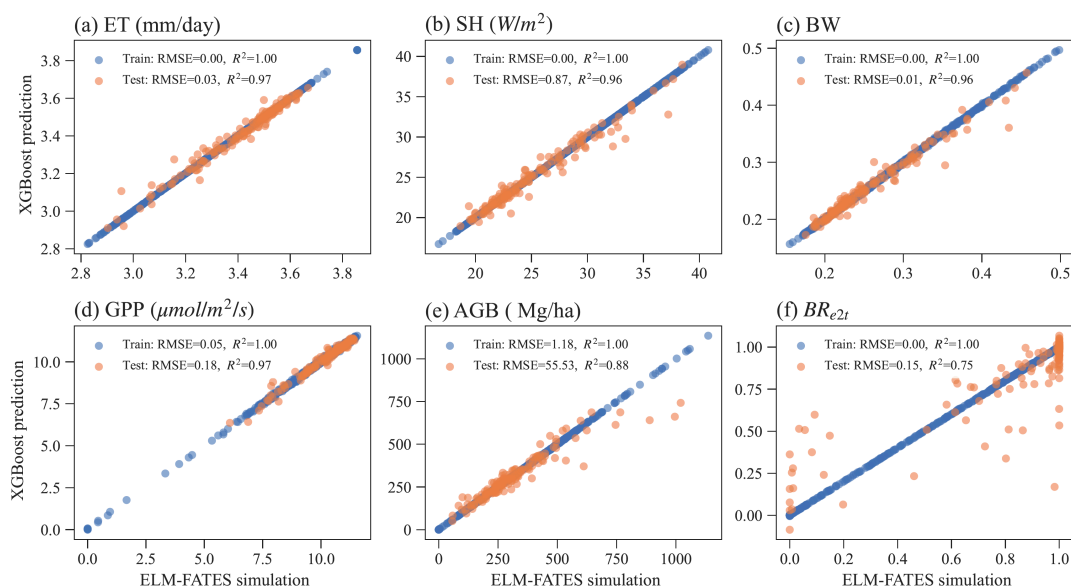


405 Figure 4. Relationships between selected parameters of Par-1. These parameters are presented in
406 three groups, i.e., green color for the late cases with $BR_{e2t} \in [0.0,0.1)$, orange color for the
407 coexisting cases with $BR_{e2t} \in [0.1,0.9]$, and blue color for the early cases with $BR_{e2t} \in (0.9,1.0]$.
408 Black star represents coexistence cases further filtered by observational constraints. (d)~(f) are the
409 corresponding kernel density estimate plots of the scatter plots (a)~(c). $V_{cmax,diff} = V_{cmax,early} -$
410 $V_{cmax,late}$. SLA_{diff} and WD_{diff} are defined likewise.

411

412 3.3 XGBoost model performance

413 Overall, the XGBoost surrogate models show good performance in predicting ELM-FATES
414 simulations (Figure 5). Based on Exp-1 (i.e., Par-1 and Out-1), six XGBoost models were trained.
415 In training, the RMSEs for the six models are zero or nearly zero, and R^2 s are close to one. In the
416 testing, four XGBoost models (i.e., XGB_ET, XGB_SH, XGB_BW, XGB_GPP) still show good
417 performance with small RMSE and large R^2 (>0.95). XGB_AGB shows a little degradation with
418 R^2 of 0.88. The performance of XGB_BR also shows degradation with R^2 decreasing from 1.0 in
419 training to 0.75 in testing. XGB_BR cannot well predict the ELM-FATES simulated BR_{e2t} of 0
420 or 1 when only one PFT survives. This indicates that PFT competition processes in ELM-FATES,
421 which determine BR_{e2t} and AGB, are highly nonlinear and difficult to emulate even using a state-
422 of-the-art machine learning algorithm.



423

424 Figure 5. The performance of XGBoost surrogate models in the training and testing for

425 predicting (a) ET, (b) SH, (c) BW, (d) GPP, (e) AGB, and (f) BR_{e2t} .

426

427 3.4 SHAP parameter importance analysis

428 Figure 6 shows the feature importance, including parameters and parameter differences, for

429 different XGBoost models. Features (on the y-axis) with a higher mean absolute SHAP value (on

430 the x-axis) denote a larger contribution to the XGBoost model prediction. The number of most

431 important features is different for predicting ET, SH, BW, and GPP compared with predicting

432 AGB and BR_{e2t} .

433 For the XGBoost models that predict ET, SH, BW, and GPP, the top three features have the largest

434 SHAP values compared to the rest (Figures 6a~5d). Notably, these top three features are the same

435 and correspond to the early successional PFT, i.e., $V_{cmax,early}$, SLA_{early} , $L_{leaf,early}$. Most ELM-

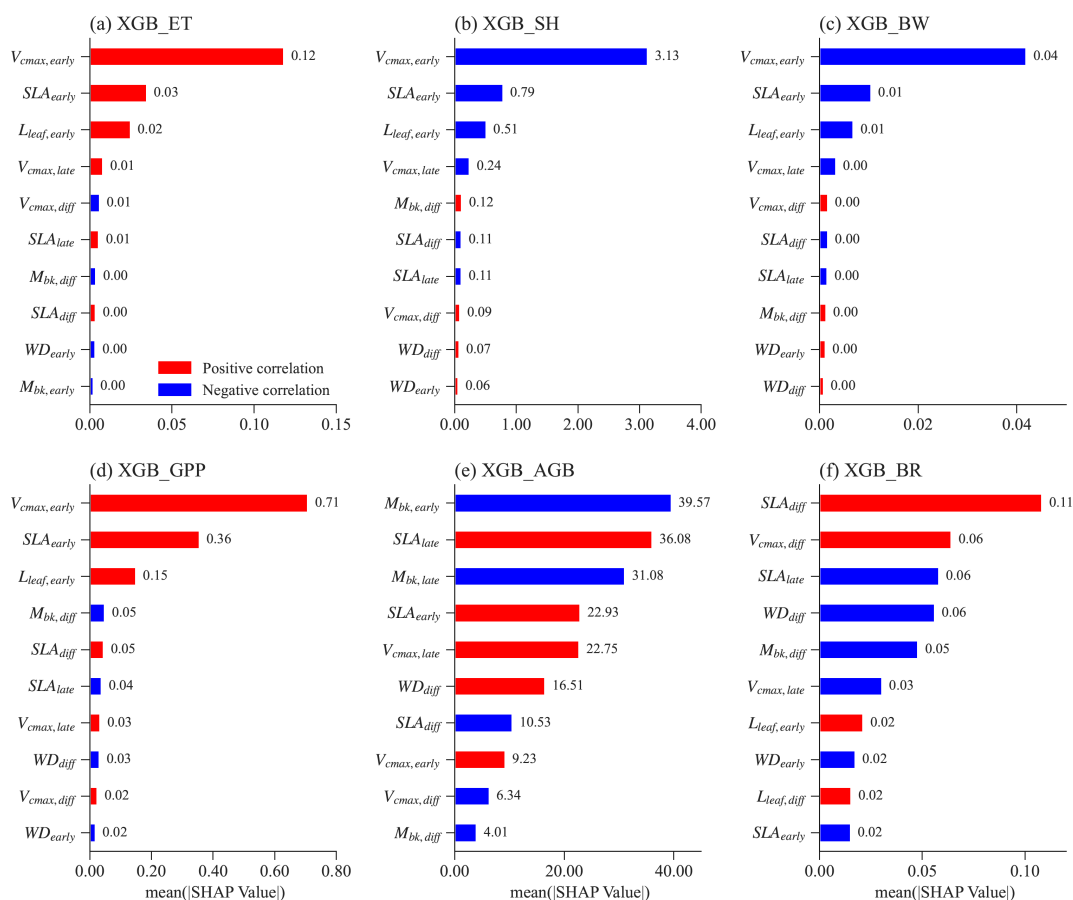
436 FATES experiments in Exp-1 used as the training samples for the XGBoost models are early cases.

437 Therefore, the parameters of early successional PFT have dominant contributions in the XGBoost



438 model predictions of overall grid-level fluxes. These three parameters are positively correlated
439 with ET and GPP and negatively correlated with SH and BW (red vs. blue bars in Figures 6a–d;
440 Figure S4 for more details), reflecting the fundamental carbon metabolism of the typically
441 dominant early successional plant.

442 For the XGBoost surrogate models of AGB and BR_{e2t} , more than eight features have large SHAP
443 values (Figures 6e and 6f). Both early and late successional PFT parameters contribute to
444 predicting the two variables. Compared with the predictions of ET, SH, BW, and GPP with only
445 three major features, predicting AGB and BR_{e2t} is relatively more complex. This is because AGB
446 and particularly BR_{e2t} are closely related to the PFT competition process in which both the early
447 and late PFT traits are crucial. Especially for BR_{e2t} , the most important features are the parameter
448 difference between the early and late successional PFTs. For example, SLA_{diff} is positively
449 correlated to BR_{e2t} . Therefore, to have coexisting PFTs with $BR_{e2t} \in [0.1, 0.9]$, the SLA of two
450 PFTs should neither be too large nor too small.



451

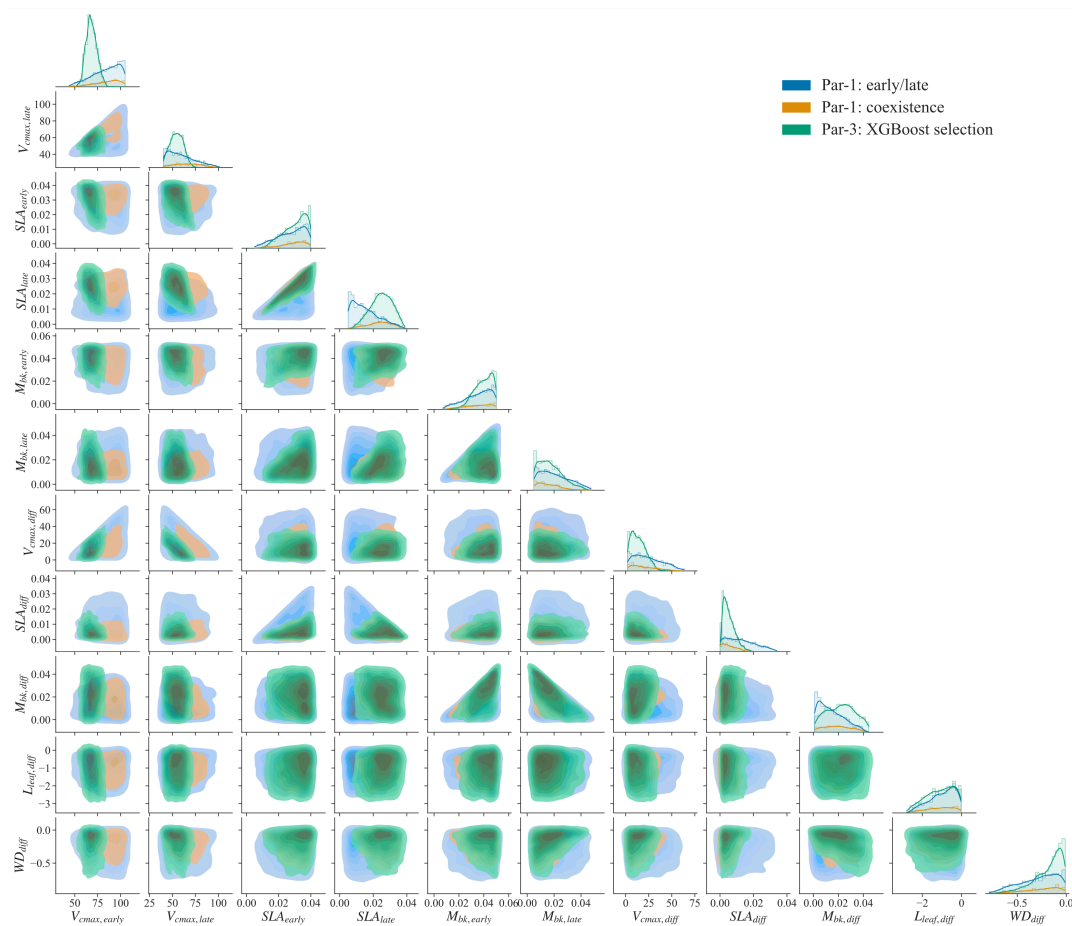
452 Figure 6. Mean absolute SHAP values for different XGBoost surrogate models for the top ten most
 453 important features. Absolute SHAP values are sorted in decreasing order from top to bottom. For
 454 each feature (y-axis) in each XGBoost model, the Spearman correlation coefficient is calculated
 455 between the feature values and the corresponding SHAP values (Figure S4). The red color means
 456 that a given feature is positively correlated with the predicting variable, whereas blue denotes a
 457 negative correlation.



458 3.5 XGBoost model parameter selection

459 Using the XGBoost surrogate models, the Par-3 ensemble was selected, including 1500 sets of
460 parameters and the corresponding parameter differences between the early and late successional
461 PFTs (Section 2.4, procedure "P4" in Figure 2). We examined whether Par-3 matches the empirical
462 relationships shown in Figure 4 (Section 3.2), i.e., $SLA_{late} > 0.35 \times SLA_{early} + 0.003$,
463 $V_{cmax,diff} < -4800 \times SLA_{diff} + 100$, and $WD_{diff} > 55 \times SLA_{diff} - 1.3$. In total, 99.1%
464 (1486 out of 1500) of parameter sets are consistent with the empirical relationships, indicating the
465 XGBoost models implicitly learned these simple relationships.

466 The parameter distributions of Par-3 show different patterns from the early/late parameters of Par-
467 1 (green vs. blue regions in Figure 7), but there are large overlaps between the coexistence
468 parameters of Par-1 and Par-3 (orange vs. green regions, e.g., the third column in Figure 7). This
469 indicates that the XGBoost surrogate models learned to select parameters around the parameters'
470 space of the coexisting cases. Par-3 also tends to have a smaller parameter difference between the
471 early and late successional PFTs in terms of SLA_{diff} and $V_{cmax,diff}$. However, Par-3 also shows
472 different patterns from the coexisting parameters of Par-1, probably because the XGBoost selected
473 parameters were also constrained by multiple observations and implicitly considered parameter
474 tradeoffs. For example, the $V_{cmax,early}$ and $V_{cmax,late}$ of Par-3 are located in narrower ranges than
475 the coexisting parameters of Par-1 (first two columns in Figure 6).



476

477 Figure 7. Comparison of parameter or parameter difference in Par-1 vs. Par-3 for eleven features.

478 The diagonal plots represent each parameter's distribution, and the rest of the subplots are kernel

479 density estimate plots. There are three groups, i.e., blue for the early/late cases of Par-1, orange for

480 the coexisting cases of Par-1, and green for Par-3 selected by XGBoost models.

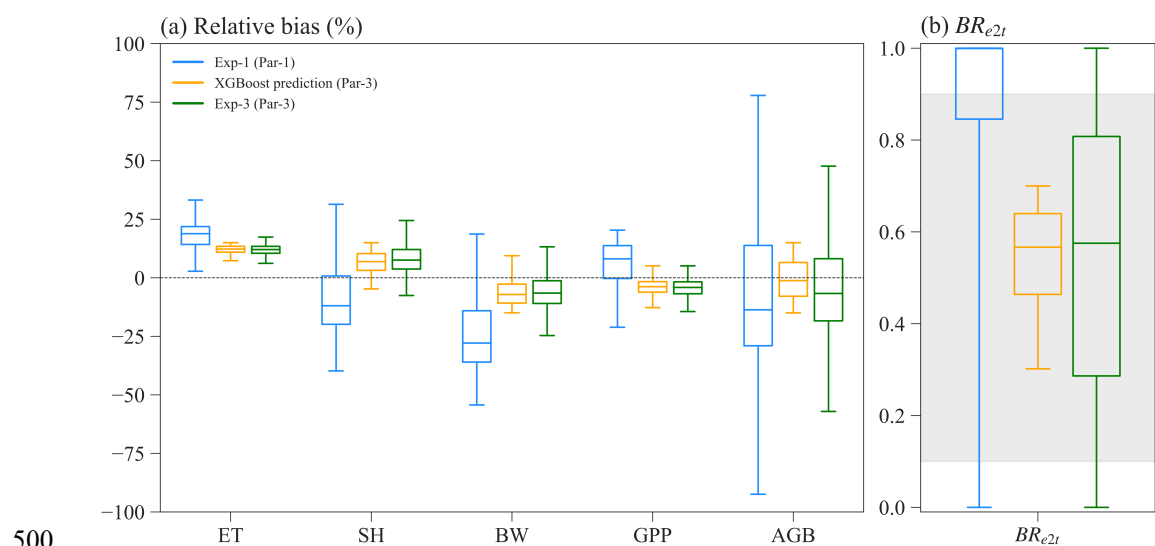
481



482 **3.6 Validation of ML selected parameters**

483 ELM-FATES simulations of Exp-3 based on the ensemble parameters of Par-3 selected by the
484 XGBoost surrogate models can better capture the observations and have more coexisting cases
485 than Exp-1 (Figure 8). The median values of simulated variables for Exp-3 are closer to
486 observations with relative biases closer to zero than Exp-1 (Figure 8a, blue vs. green boxes). The
487 Exp-3 simulated variables also have more concentrated distributions than Exp-1. Compared to the
488 skewed distribution of BR_{e2t} in Exp-1 with a large proportion of early cases, Exp-3 has a more
489 normally distributed BR_{e2t} (Figure 8b). Specifically, Exp-3 has about 3.6 times more coexisting
490 cases than Exp-1, i.e., 73.1% (1097 out of 1500) in Exp-3 vs. 20.6% (309 out of 1500) in Exp-1
491 (Table S3). After being further constrained by observation (Table S3), one-third of the experiments
492 (i.e., 495 out of 1500) in Exp-3 remain, and this ratio is 23.6 times more than 1.4% (21 out of 1500)
493 in Exp-1.

494 The XGBoost surrogate model predicted variables also match well with those simulated using
495 ELM-FATES in Exp-3 (Figure 8, orange vs. green boxes), indicating the overall reasonable
496 accuracy for the XGBoost model predictions. Compared to the ELM-FATES results using Par-3,
497 the XGBoost models show better performance for ET, SH, BW, and GPP, but relatively degraded
498 performance for AGB and BR_{e2t} (Figure S5). It is consistent with the performance of the XGBoost
499 models' training and testing results (in Section 3.3).



500

501 Figure 8. Comparison between the ELM-FATES simulations for Exp-1 and Exp-3. (a) Relative
 502 bias for simulated ET, SH, BW, GPP, and AGB. (b) Simulated BR_{e2t} . XGBoost prediction
 503 represents the selected XGBoost model predictions after filtering with observation and biomass
 504 ratio (i.e., the XGB_prds, procedure "P4" in Figure 2).

505

506 3.7 Parameter tradeoff for coexisting experiments

507 Parameters of the early and late successional PFTs show tradeoffs for the coexisting experiments.

508 Large relative differences in SLA , V_{cmax} , and WD (more negative) favor the early successional

509 PFT, while large relative differences in M_{bk} and L_{leaf} favor the late successional PFT. Therefore,

510 in Exp-1, compared to the early and late cases, the coexisting cases have intermediate relative

511 differences in SLA , V_{cmax} , WD , M_{bk} and L_{leaf} (dashed boxes in Figure 9). The coexisting cases

512 in Exp-3 have similar patterns with intermediate relative differences in SLA , V_{cmax} and L_{leaf}

513 compared to the early and late cases (solid boxes in Figure 9). However, M_{bk} and especially WD

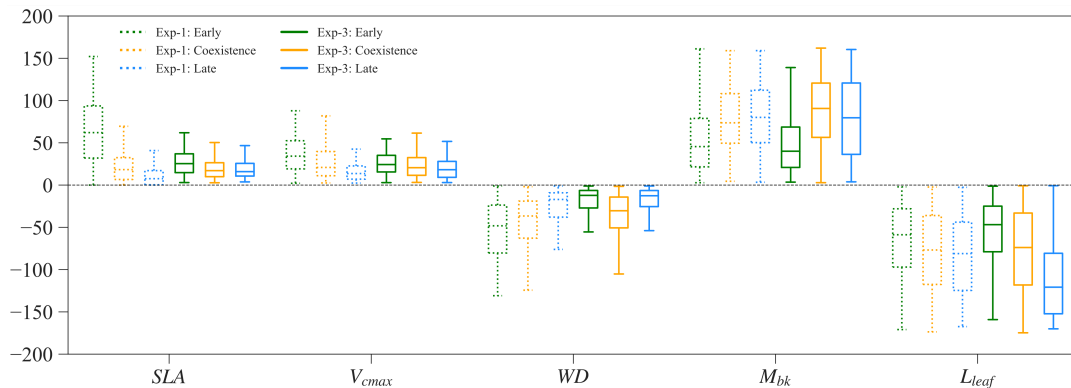
514 show the largest relative difference for the coexisting cases compared to the early and late cases



515 in Exp-3. These two parameters still show a tradeoff in determining coexisting PFTs, because
 516 larger WD favors the early PFT while larger M_{bk} favors the late PFT.

517

518 In Exp-3, the parameter spaces of the coexisting cases show large overlaps with the early/late cases
 519 (Figure S6). There are no simple correlations between these parameters to distinguish the
 520 coexisting cases from the early and late cases (also see Section 3.2). Although WD_{diff} of the
 521 coexisting cases still overlap with the early/late cases, when WD_{diff} is less than roughly -0.4
 522 (g/cm^3), only coexisting cases exist (Figure S6). Nevertheless, this rule (i.e., $WD_{diff} < -0.4$) alone
 523 cannot ensure PFT coexistence (see Figure 7).



524

525 Figure 9. Parameter relative difference (%) between early successional PFT and late successional
 526 PFT for Exp-1 (box with dash line) and Exp-3 (box with solid line). Parameter relative difference

527 is calculated as, taking SLA as an example, $\frac{SLA_{early} - SLA_{late}}{(SLA_{early} + SLA_{late})/2} \times 100$ (%).

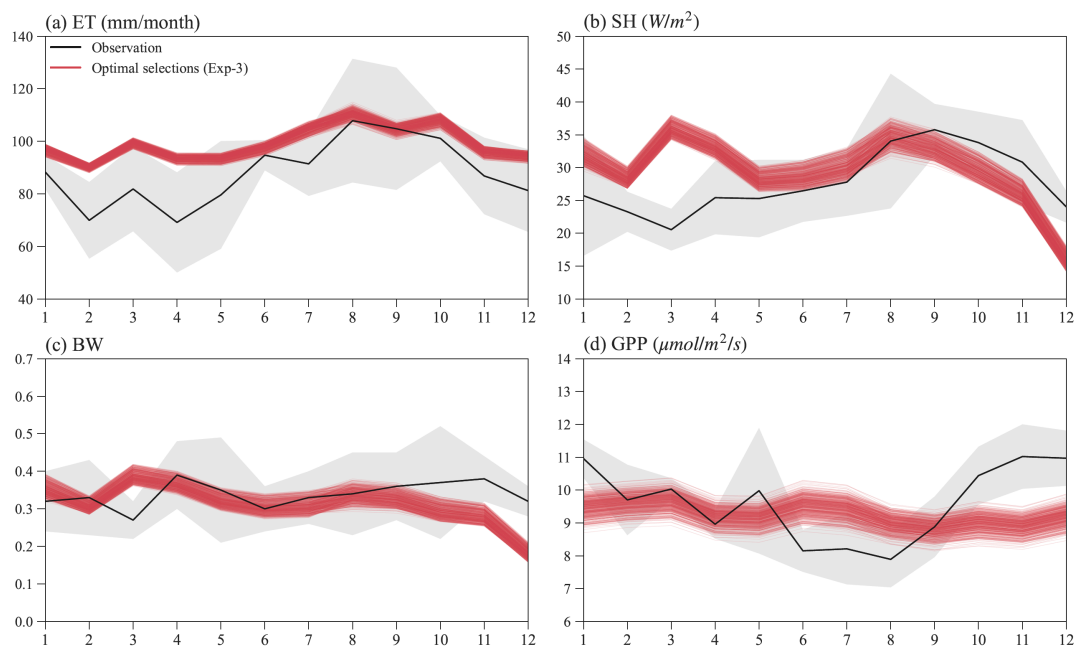
528

529



530 **3.8 Seasonal variation comparison**

531 Figure 10 shows the seasonal variations of ET, SH, BW, and GPP for observations and simulations
532 of the finally selected 495 experiments in Exp-3 with good model performance (Table S3). Overall,
533 the simulated ET shows a similar seasonal variation to ET observation (Figure 10a), with relatively
534 small ET in the wet season (November–May), high ET in the dry season (June–October), and ET
535 peaks in August. However, compared to the observations, ELM-FATES overestimates ET,
536 especially during the wet season. The simulated SH also shows a similar seasonal variation with
537 the SH observation except in March. ELM-FATES overestimated SH from January to May but
538 underestimated SH from September to December (Figure 10b). Due to the discrepancy between
539 simulated ET and SH, the model underestimates BW from September to December (Figure 10c).
540 The simulated GPP has minor seasonal variability compared to the observed GPP. ELM-FATES
541 overestimates GPP from June–August in the dry season, but underestimates GPP over October–
542 December. The lower GPP over June–August indicates that plants may be relatively water-stressed
543 or energy limited during these months. However, the large ET observation over the same period
544 implies that this site is unlikely water limited or strongly energy limited. The ELM-FATES
545 simulations also display little water stress year-round (Figure S7). Therefore, there are likely
546 elements of the seasonal cycle (e.g., phenological responses of photosynthetic capacity) that are
547 not yet captured here. Additionally, tower estimates of GPP may also have large uncertainties.



548

549 Figure 10. Mean monthly observations and selected optimal ELM-FATES simulations in Exp-3
550 for (a) ET, (b) SH, (c) BW, and (d) GPP. Each red line represents one experiment simulation (four-
551 year simulation average). The black curves are monthly climatologic averages from 2000 to 2008,
552 and the grey shaded area represents the interannual variabilities (i.e., *mean \pm*
553 *standard deviation*).

554



555 **4. Discussion**

556 **4.1 Limited guidance of observed trait relationships for PFT coexistence modeling in FATES**

557 We found degraded PFT coexistence in ELM-FATES simulation when observed trait relationships
558 are considered. More specifically, constrained by observed trait relationships, Exp-2 has fewer
559 coexisting cases than Exp-1 which does not consider the observed trait relationships. The observed
560 trait relationships were derived from site measurements in the species-rich tropical ecosystem
561 where plant coexistence commonly happens (Kraft et al., 2008), which is expected to enhance the
562 PFT coexistence simulations. This inconsistency could be due to several possible reasons. First,
563 ELM-FATES is a typical "trait filtering" model (Fisher et al., 2018), and the realistic simulation
564 of PFT dynamics largely depends on the fidelity with which trait tradeoff surfaces are prescribed
565 in the model (Scheiter et al., 2012). Implicit representation of trait tradeoff in the current ELM-
566 FATES model may not be well balanced, which may differ from the observed trait relationships
567 that lead to coexistence in the real world (at least for the ecosystem at our study site). In particular,
568 there may be correlated tradeoffs that are unmeasured (e.g., with below ground processes, Chitra-
569 Tarak et al. 2021) but not represented in the model. A second reason could be the mismatch
570 between different spatial scales. The observed trait relationships are derived from field
571 measurements across tropical forests over a large region with diverse species and climate, e.g., the
572 relationship in equation (1) is for plant species in Panama. In contrast, ELM-FATES simulations
573 were conducted at the K34 site scale with specific species composition. Therefore, the large-scale
574 trait relationships may not reflect the small-scale trait relationships. Wright et al. (2005) showed
575 that trait relationships fitted for individual sites varied considerably. Third, the observed trait
576 relationships are based on simplified equations, which may not be able to comprehensively reflect
577 PFT coexistence. For example, although equation (2) derived from Longo et al. (2020) can reflect



578 the negative relationship between SLA and L_{leaf} , the R^2 of this equation is about 0.49, which may
579 not be accurate enough to represent trait relationships. Additionally, these equations (1)~(3) do not
580 consider the uncertainty of traits covariance. In Koven et al. (2020), the uncertainties between trait
581 covariance were considered when sampling parameters for FATES experiments, which may be
582 considered in future studies.

583

584 **4.2 Advantages of ML surrogate models on improving PFT coexistence modeling**

585 ELM-FATES simulations driven by parameters selected using the XGBoost models essentially
586 improved PFT coexistence and better captured observations. Compared to the initial Exp-1, which
587 was used to train the XGBoost models, the proportion of coexisting PFTs in Exp-3 reaches 73.1%,
588 3.6 times more than 20.6% in Exp-1. Further filtering the coexistence experiments by observations,
589 Exp-3 still has 33.0% of experiments left with good model performance, 23.6 times that of 1.4%
590 of experiments in Exp-1 with good performance. Our ML-based approach also outperforms the
591 empirical correlations built in Section 3.2, which only yields 32.5% of coexistence experiments
592 and this reduces to 2.3% of experiments if further constrained by observation. The large proportion
593 of optimal experiments selected by our ML approach also outperforms previous studies using
594 direct filtering approaches. Buotte et al. (2021) conducted two stages of experiments to select
595 optimal parameters for CLM-FATES modeling with two conifer species; only 0.3% (1 out of 360)
596 of the cases met the given criteria in the first stage experiments, which increased to 5.5% in the
597 second stage experiments. Huang et al. (2020) conducted CLM-FATES modeling with two
598 tropical PFTs at the Tapajós National Forest sites; only one parameter set out of seventy (about
599 1.4%) was selected with reasonable fractions of two PFTs and minor errors compared to
600 observations. In addition, the parameter selection procedures of these two studies require some



601 degree of subjective decision making and expert knowledge. On the other hand, our ML-based
602 approach takes a more objective procedure, and little expert knowledge is required except for the
603 initial determination of the parameter reference ranges. Importantly, we believe this approach can
604 be repeatable as, e.g., model developments lead to changes between the parameter values and
605 model predictions of forest structure and function, and can be used to define constrained ensemble
606 values that will allow assessment of confidence in model predictions. Even though simulating
607 coexistence of different plants may not be a big concern for individual-based DGVMs , e.g.,
608 LPJmL-FIT (Sakschewski et al., 2015, 2016) and TROLL (Maréchaux and Chave, 2017), our
609 approach also could be applied to the selection of key parameters that regulate vegetation dynamics
610 in these models.

611

612 Our study also reproduced the observations satisfactorily. Holm et al. (2020) conducted the ELM-
613 FATES simulation with only one PFT considered at the same K34 site. Our study yields better or
614 similar performance in the magnitude of AGB, and the magnitude and seasonal variation of GPP,
615 ET, SH, and BW (Table 2 and Figure 3 in Holm et al. 2020 vs. Figures 8 and 10 in this study). It
616 should also be noted that the overestimation of simulated energy fluxes (latent heat and SH) from
617 January to May could be associated with the energy-related processes (e.g., energy partition,
618 surface albedo) in ELM-FATES. Other potential reasons could be related to the uncertainties in
619 atmospheric forcing and the common issue of incomplete energy budget closure at eddy covariance
620 towers (Wilson et al., 2002; Foken, 2008; Rocha et al., 2009).

621

622 Compared to the predictions of GPP, ET, SH, and BW simulated by ELM-FATES, the XGBoost
623 surrogate models show slightly degraded performance in predicting the simulated BR_{e2t} and AGB



624 (Figures 5 and S5). Three parameters ($V_{cmax,early}$, SLA_{early} , and $L_{leaf,early}$) mainly control the
625 predictions of ET, SH, BW, and GPP, while eight features are crucial for predicting AGB and
626 BR_{e2t} . Even though the XGBoost algorithm has an excellent ability to capture complex nonlinear
627 relationships, it does not predict well the PFT competition related variables of AGB and BR_{e2t}
628 because the physical model cannot robustly predict coexisting PFTs due to the higher
629 dimensionality of predicting PFT composition as compared to other ecosystem variables.
630 Therefore, even though the XGBoost surrogate models essentially improve plant coexistence
631 modeling, further studies are still needed to improve the emulation of PFT competition related
632 variables. Other approaches that have been applied in DGVMs but not specifically for PFT
633 coexistence modeling, for example, the generalized likelihood uncertainty estimation (GLUE)
634 approach (Zhang et al., 2022) and the Bayesian model emulation approach (Fer et al., 2018), could
635 provide alternative ways. Additionally, the adoption of deep learning algorithms and the
636 consideration of additional mechanisms in FATES are also advocated.

637

638 **4.3 Trait tradeoffs between coexisting PFTs**

639 Trait-related parameters show tradeoffs between early and late successional PFTs for the ELM–
640 FATES simulated coexisting experiments. The relative differences between the two PFTs in SLA ,
641 V_{cmax} , and WD complementarily coordinate with the relative difference in M_{bk} and L_{leaf} , hence
642 avoiding competitive exclusion (Figure 9). These ELM-FATES reflected tradeoffs are consistent
643 with the niche-based species coexistence mechanisms of environmental filtering and niche
644 partitioning (MICHALKO and PEKÁR, 2015; Adler et al., 2013). On the one hand, in the
645 coexisting cases, the relative differences between the two PFTs' parameters should not be
646 considerable. For example, a large difference in SLA more likely favors the early cases (green



647 dash box in Figure 9). This is related to environmental filtering in which coexisting species require
648 some degree of convergence in strategy to survive and persist under given environmental
649 conditions (Cadotte and Tucker, 2017; Thakur and Wright, 2017). On the other hand, some degree
650 of differences should exist between the two PFTs' parameters in the coexisting cases. This is
651 related to niche partitioning to ensure either difference in resource requirements or differences in
652 tolerance to surrounding conditions (Kraft et al., 2015; Fowler et al., 2013). Phenomenological
653 evidence has shown that functional trait variation promotes coexistence or increases species
654 richness (Uriarte et al., 2010; Angert et al., 2009; Adler et al., 2006; Mason et al., 2012; Ben-Hur
655 et al., 2012).

656

657 In our ELM-FATES simulations, the primary axis of competition for resources is light. The
658 tradeoffs between the two PFTs' parameters differentiate their vertical competition in light
659 absorption, which has been shown to strongly control tropical forest community composition
660 (Farrion et al., 2016; Poorter et al., 2003). Even though the early PFT has a shallower rooting depth
661 than the late PFT, there is no critical dry condition during our simulation period (i.e., corresponding
662 to values of the water stress factor (BTRAN) close to 1.0 in Figure S7). Therefore, competition for
663 water resource access negligibly contributes to PFT coexistence in this study. Previous tropical
664 studies also revealed these coexistence mechanisms. At a tropical forest site in eastern Ecuador,
665 Kraft et al. (2008) found that cooccurring trees are often less ecologically similar, and both
666 environmental filtering (different topographic habitats of ridgetops vs. valley) and niche
667 differentiation simultaneously contribute to species coexistence. Swenson & Enquist (2009) also
668 found that at small spatial scales in a tropical forest, most traits of coexisting species were under-



669 dispersed, consistent with environmental filtering, while the seed mass and maximum height were
670 over-dispersed, reflecting niche partitioning.

671

672 **4.4 Limitations and further model development**

673 Some limitations exist in our experiments. Niche partitioning is a critical aspect of promoting
674 species coexistence, which is closely related to spatial heterogeneity, temporal heterogeneity,
675 disturbances (e.g., nature enemy, fire), and resource partitioning (Adler et al., 2013). In our current
676 ELM-FATES simulations, some processes that have been or are being developed in the model are
677 not considered. These processes include nutrient limitation (Holm et al., 2020), fire disturbance
678 (Fisher et al., 2015), subsurface lateral flow (Fang et al., 2022), and plant hydraulics (Chitra-Tarak
679 et al., 2021; Li et al., 2021). Ignoring these processes could limit the potential of niche partitioning
680 among PFT in our ELM-FATES simulations. Topography has been recognized as an essential
681 spatial heterogeneity factor for tropical forests, but it is not considered in ELM-FATES (Kraft et
682 al., 2008; Costa et al., 2022). For example, Fang et al. (2022) coupled a three-dimensional
683 hydrology model (ParFlow) with ELM-FATES and found that lateral flow plays a prominent role
684 in governing aboveground biomass, and Cheng et al. (2021) also found a critical role for subsurface
685 hydrology on coexistence. As these processes are added to the model, the reproducibility aspects
686 of the XGBoost method to identify PFT combinations that match a broad range of criteria will be
687 particularly important.

688 Lacking other features or processes could also affect PFTs coexistence in the current FATES. For
689 example, plant trait plasticity, that plants can adjust their morphological and/or physiological traits
690 to better adapt to the environment (Nicotra et al., 2010; Bloomfield et al., 2018; McDowell et al.,
691 2022), is also not well considered in FATES. Leaf traits such as V_{cmax} and SLA do vary vertically



692 through the canopy in FATES, via a prescribed relationship described by Lloyd et al., 2010. Liu
693 and Ng (2019) found that the SLA of a desert shrubland is significantly correlated with seasonal
694 water availability. Additionally, FATES only considers the inter-PFT variance of functional traits
695 (e.g., different V_{cmax} for early and late PFT). However, studies revealed that trait variations
696 commonly exist within and between species (Wright et al., 2005; Engemann et al., 2016; Meng et
697 al., 2015; Dong et al., 2020; Siefert et al., 2015), which play a vital role in maintaining plant
698 diversity (Violle et al., 2012; Lu et al., 2017). Reproductive features that enhance competitive
699 exclusion tendencies have been illustrated to affect coexistence (Maréchaux and Chave, 2017;
700 Fisher et al., 2018). Hanbury-Brown et al. (2022) discussed the importance of the representation
701 of forest regeneration, including improving parameters and algorithms for reproductive allocation,
702 dispersal, seed survival and germination, environmental filtering in the seedling layer, and tree
703 regeneration strategies adapted to wind, fire, and anthropogenic disturbance regimes. Besides, both
704 growth-survival and stature-recruitment tradeoffs are critical to accurately predict successional
705 patterns in tropical forest structure and competition (see details in Rüger et al., 2020), which should
706 also be better considered in future model development. Furthermore, measured plant traits are
707 increasingly available, e.g., the TRY datasets (Kattge et al., 2020) can be used to improve the
708 model process and parameterizations. Future studies on properly and adequately using these
709 datasets to guide DGVMs parameterizations are advocated.



710 **5. Conclusions**

711 In this study, we explored two possible solutions to improve PFT coexistence modeling in a cohort-
712 based model (ELM-FATES): (1) using plant trait relationships established from field
713 measurements and (2) using machine learning based surrogate models to optimize parameters.
714 Multiple ensembles of ELM-FATES experiments were conducted over a tropical forest site at
715 Manaus, Brazil. We found that considering the observed trait relationships (Exp-2) slightly
716 improves the simulations of water (ET), energy (SH and BW), and carbon (GPP, AGB) variables
717 when compared against observations, but degrades the simulation of PFT coexistence. Based on
718 Exp-1, the XGBoost surrogate models were built to optimize the ELM-FATES parameters by
719 integrating the observations (i.e., ET, SH, BW, GPP, and AGB) and PFT coexistence criteria (i.e.,
720 PFT biomass ratio). Exp-3 with parameters selected by the ML-surrogate models vastly improves
721 the ELM-FATES simulation of PFT coexistence, and also better reproduces the annual means and
722 seasonal variations of ET, SH, BW, GPP, and the field inventory of AGB. This study demonstrates
723 the benefits of using machine learning models to improve the modeling of PFT coexistence in
724 ELM-FATES and modeling of tropical forest environments, with important implications for
725 modeling the response and feedback of ecosystem dynamics to climate change. Our results also
726 suggest that adding additional mechanisms of species competition in FATES is also critical for
727 robust modeling of coexisting PFTs.

728



729 *Code and Data Availability.* The ELM-FATES source code, related surface and domain data, and
730 forcing data used in this study are archived on Zenodo (Li et al., 2022,
731 <https://doi.org/10.5281/zenodo.7319876>). The observational reference datasets of GPP, ET, SH,
732 BW, and AGB are obtained from Holm et al. (2020). The forcing data is available from Oak
733 Ridge National Laboratory Distributed Active Archive Center (ORNL DAAC), LBA-ECO CD-
734 32 Flux Tower Network Data Compilation, Brazilian Amazon: 1999-2006, V2,
735 https://daac.ornl.gov/LBA/guides/CD32_Fluxes_Brazil.html.
736

737 *Author contributions.* LL and YF designed and conducted the experiments, analyzed model
738 outputs, and drafted the manuscript. ZZ and MS contributed to the machine learning, experiment
739 design, and improvement of the manuscript. LRL contributed to the interpretation and discussion
740 of results, and improvement of the manuscript. ML, CDK, JAH, RAF, NGM, and JC contributed
741 to the dataset, interpretation and discussion of the results, and modification of the manuscript.
742

743 *Acknowledgments.* This research was conducted at Pacific Northwest National Laboratory,
744 operated for the U.S. Department of Energy by Battelle Memorial Institute under contract DE-
745 AC05-76RL01830. This study was supported by the Department of Energy's (DOE) Office of
746 Biological and Environmental Research as part of the Terrestrial Ecosystem Science program
747 through the Next-Generation Ecosystem Experiments (NGEE)-Tropics project.
748

749 *Financial support.* This research was supported by the U.S. Department of Energy, Office of
750 Science (grant no. 71073).

751 *Competing interests.* The authors declare that they have no conflict of interest.



752 Reference

753

- 754 Adler, P. B., HilleRisLambers, J., Kyriakidis, P. C., Guan, Q., and Levine, J. M.: Climate
755 variability has a stabilizing effect on the coexistence of prairie grasses., *P Natl Acad Sci Usa*,
756 103, 12793–8, <https://doi.org/10.1073/pnas.0600599103>, 2006.
- 757 Adler, P. B., Fajardo, A., Kleinhesselink, A. R., and Kraft, N. J. B.: Trait-based tests of
758 coexistence mechanisms, *Ecol Lett*, 16, 1294–1306, <https://doi.org/10.1111/ele.12157>, 2013.
- 759 Angert, A. L., Huxman, T. E., Chesson, P., and Venable, D. L.: Functional tradeoffs determine
760 species coexistence via the storage effect, *Proc National Acad Sci*, 106, 11641–11645,
761 <https://doi.org/10.1073/pnas.0904512106>, 2009.
- 762 Antoniadis, A., Lambert-Lacroix, S., and Poggi, J.-M.: Random forests for global sensitivity
763 analysis: A selective review, *Reliab Eng Syst Safe*, 206, 107312,
764 <https://doi.org/10.1016/j.ress.2020.107312>, 2020.
- 765 Bauman, D., Fortunel, C., Delhaye, G., Malhi, Y., et al.: Tropical tree mortality has increased
766 with rising atmospheric water stress, *Nature*, 1–6, <https://doi.org/10.1038/s41586-022-04737-7>,
767 2022.
- 768 Ben-Hur, E., Fragman-Sapir, O., Hadas, R., Singer, A., and Kadmon, R.: Functional trade-offs
769 increase species diversity in experimental plant communities, *Ecol Lett*, 15, 1276–1282,
770 <https://doi.org/10.1111/j.1461-0248.2012.01850.x>, 2012.
- 771 Berzaghi, F., Wright, I. J., Kramer, K., Oddou-Muratorio, S., Bohn, F. J., Reyer, C. P. O.,
772 Sabaté, S., Sanders, T. G. M., and Hartig, F.: Towards a New Generation of Trait-Flexible
773 Vegetation Models, *Trends Ecol Evol*, 35, 191–205, <https://doi.org/10.1016/j.tree.2019.11.006>,
774 2019.
- 775 Bloomfield, K. J., Cernusak, L. A., Eamus, D., Ellsworth, D. S., et al.: A continental-scale
776 assessment of variability in leaf traits: Within species, across sites and between seasons, *Funct*
777 *Ecol*, 32, 1492–1506, <https://doi.org/10.1111/1365-2435.13097>, 2018.
- 778 Bonan, G. B.: Forests and Climate Change: Forcings, Feedbacks, and the Climate Benefits of
779 Forests, *Science*, 320, 1444–1449, <https://doi.org/10.1126/science.1155121>, 2008.
- 780 Brister, E., Newhouse, A. E., and Texas, C. for E. P., The University of North: Not the Same Old
781 Chestnut: Rewilding Forests with Biotechnology, *Environ Ethics*, 42, 149–167,
782 <https://doi.org/10.5840/enviroethics2020111614>, 2020.
- 783 Buotte, P. C., Koven, C. D., Xu, C., Shuman, J. K., Goulden, M. L., Levis, S., Katz, J., Ding, J.,
784 Ma, W., Robbins, Z., and Kueppers, L. M.: Capturing functional strategies and compositional
785 dynamics in vegetation demographic models, *Biogeosciences*, 18, 4473–4490,
786 <https://doi.org/10.5194/bg-18-4473-2021>, 2021.



- 787 Cadotte, M. W. and Tucker, C. M.: Should Environmental Filtering be Abandoned?, *Trends Ecol*
788 *Evol*, 32, 429–437, <https://doi.org/10.1016/j.tree.2017.03.004>, 2017.
- 789 Cao, M. and Woodward, F. I.: Dynamic responses of terrestrial ecosystem carbon cycling to
790 global climate change, *Nature*, 393, 249–252, <https://doi.org/10.1038/30460>, 1998.
- 791 Chen, T. and Guestrin, C.: XGBoost: A Scalable Tree Boosting System, *Proc 22nd Acm Sigkdd*
792 *Int Conf Knowl Discov Data Min*, 785–794, <https://doi.org/10.1145/2939672.2939785>, 2016.
- 793 Cheng, Y., Leung, L. R., Huang, M., Koven, C., Detto, M., Knox, R., Bisht, G., Bretfeld, M., and
794 Fisher, R. A.: Modeling the joint effects of vegetation characteristics and soil properties on
795 ecosystem dynamics in a Panama tropical forest, *J Adv Model Earth Sy*,
796 <https://doi.org/10.1029/2021ms002603>, 2021.
- 797 Chitra-Tarak, R., Xu, C., Aguilar, S., Anderson-Teixeira, K. J., Chambers, J., Detto, M.,
798 Faybishenko, B., Fisher, R. A., Knox, R. G., Koven, C. D., et al.: Hydraulically-vulnerable trees
799 survive on deep-water access during droughts in a tropical forest, *New Phytol*, 231, 1798–1813,
800 <https://doi.org/10.1111/nph.17464>, 2021.
- 801 Christoffersen, B. O., Gloor, M., Fauset, S., Fyllas, N. M., Galbraith, D. R., Baker, T. R., Kruijt,
802 B., Rowland, L., Fisher, R. A., Binks, O. J., Sevanto, S., Xu, C., Jansen, S., Choat, B.,
803 Mencuccini, M., McDowell, N. G., and Meir, P.: Linking hydraulic traits to tropical forest
804 function in a size-structured and trait-driven model (TFS v.1-Hydro), *Geoscientific Model*
805 *Development*, 9, 4227–4255, <https://doi.org/10.5194/gmd-9-4227-2016>, 2016.
- 806 Costa, F. R. C., Schiatti, J., Stark, S. C., and Smith, M. N.: The other side of tropical forest
807 drought: do shallow water table regions of Amazonia act as large-scale hydrological refugia from
808 drought?, *New Phytol*, <https://doi.org/10.1111/nph.17914>, 2022.
- 809 Dagon, K., Sanderson, B. M., Fisher, R. A., and Lawrence, D. M.: A machine learning approach
810 to emulation and biophysical parameter estimation with the Community Land Model, version 5,
811 *Adv Statistical Clim Meteorology Oceanogr*, 6, 223–244, [https://doi.org/10.5194/ascmo-6-223-](https://doi.org/10.5194/ascmo-6-223-2020)
812 [2020](https://doi.org/10.5194/ascmo-6-223-2020), 2020.
- 813 Díaz, S., Kattge, J., Cornelissen, J. H. C., Wright, I. J., Lavorel, S., Dray, S., Reu, B., Kleyer, M.,
814 Wirth, C., Prentice, I. C., Garnier, E., Bönsch, G., et al.: The global spectrum of plant form and
815 function, *Nature*, 529, 167–171, <https://doi.org/10.1038/nature16489>, 2016.
- 816 Domingues, T. F., Berry, J. A., Martinelli, L. A., Ometto, J. P. H. B., and Ehleringer, J. R.:
817 Parameterization of Canopy Structure and Leaf-Level Gas Exchange for an Eastern Amazonian
818 Tropical Rain Forest (Tapajós National Forest, Pará, Brazil), *Earth Interact*, 9, 1–23,
819 <https://doi.org/10.1175/ei149.1>, 2005.
- 820 Dong, N., Prentice, I. C., Wright, I. J., Evans, B. J., Togashi, H. F., Caddy-Retalic, S.,
821 McInerney, F. A., Sparrow, B., Leitch, E., and Lowe, A. J.: Components of leaf-trait variation



- 822 along environmental gradients, *New Phytol*, 228, 82–94, <https://doi.org/10.1111/nph.16558>,
823 2020.
- 824 Duan, Q., Sorooshian, S., and Gupta, V.: Effective and efficient global optimization for
825 conceptual rainfall-runoff models, *Water Resour Res*, 28, 1015–1031,
826 <https://doi.org/10.1029/91wr02985>, 1992.
- 827 Engemann, K., Sandel, B., Boyle, B., Enquist, B. J., Jørgensen, P. M., Kattge, J., McGill, B. J.,
828 Morueta-Holme, N., Peet, R. K., Spencer, N. J., Violle, C., Wisser, S. K., and Svenning, J.-C.: A
829 plant growth form dataset for the New World., *Ecology*, 97, 3243–3243,
830 <https://doi.org/10.1002/ecy.1569>, 2016.
- 831 Fang, Y., Leung, L. R., Duan, Z., Wigmosta, M. S., Maxwell, R. M., Chambers, J. Q., and
832 Tomasella, J.: Influence of landscape heterogeneity on water available to tropical forests in an
833 Amazonian catchment and implications for modeling drought response, *Journal of Geophysical*
834 *Research: Atmospheres*, 122, 8410–8426, <https://doi.org/10.1002/2017jd027066>, 2017.
- 835 Fang, Y., Leung, R., Koven, C., Bisht, G., Detto, M., Cheng, Y., McDowell, N., Muller-Landau,
836 H., Wright, S. J., and Chambers, J.: Modeling the topographic influence on aboveground
837 biomass using a coupled model of hillslope hydrology and ecosystem dynamics, *Geoscientific*
838 *Model Dev Discuss*, 2022, 1–41, <https://doi.org/10.5194/gmd-2022-148>, 2022.
- 839 Farrior, C. E., Bohlman, S. A., Hubbell, S., and Pacala, S. W.: Dominance of the suppressed:
840 Power-law size structure in tropical forests, *Science*, 351, 155–157,
841 <https://doi.org/10.1126/science.aad0592>, 2016.
- 842 Feeley, K. J., Davies, S. J., Ashton, P. S., Bunyavejchewin, S., Supardi, M. N. N., Kassim, A. R.,
843 Tan, S., and Chave, J.: The role of gap phase processes in the biomass dynamics of tropical
844 forests, *Proc Royal Soc B Biological Sci*, 274, 2857–2864,
845 <https://doi.org/10.1098/rspb.2007.0954>, 2007.
- 846 Feigl, M., Lebedzinski, K., Herrnegger, M., and Schulz, K.: Machine-learning methods for
847 stream water temperature prediction, *Hydrol Earth Syst Sc*, 25, 2951–2977,
848 <https://doi.org/10.5194/hess-25-2951-2021>, 2021.
- 849 Fer, I., Kelly, R., Moorcroft, P. R., Richardson, A. D., Cowdery, E. M., and Dietze, M. C.:
850 Linking big models to big data: efficient ecosystem model calibration through Bayesian model
851 emulation, *Biogeosciences*, 15, 5801–5830, <https://doi.org/10.5194/bg-15-5801-2018>, 2018.
- 852 Fisher, R., McDowell, N., Purves, D., Moorcroft, P., Sitch, S., Cox, P., Huntingford, C., Meir, P.,
853 and Woodward, F. I.: Assessing uncertainties in a second-generation dynamic vegetation model
854 caused by ecological scale limitations, *New Phytol*, 187, 666–681,
855 <https://doi.org/10.1111/j.1469-8137.2010.03340.x>, 2010.
- 856 Fisher, R. A., Muszala, S., Versteinstein, M., Lawrence, P., Xu, C., McDowell, N. G., Knox, R.
857 G., Koven, C., Holm, J., Rogers, B. M., Spessa, A., Lawrence, D., and Bonan, G.: Taking off the



- 858 training wheels: the properties of a dynamic vegetation model without climate envelopes,
859 CLM4.5(ED), Geosci Model Dev, 8, 3593–3619, <https://doi.org/10.5194/gmd-8-3593-2015>,
860 2015.
- 861 Fisher, R. A., Koven, C. D., Anderegg, W. R. L., Christoffersen, B. O., Dietze, M. C., Farrior, C.
862 E., Holm, J. A., Hurtt, G. C., Knox, R. G., Lawrence, P. J., et al.: Vegetation demographics in
863 Earth System Models: A review of progress and priorities, Global Change Biol, 24, 35–54,
864 <https://doi.org/10.1111/gcb.13910>, 2018.
- 865 Foken, T.: THE ENERGY BALANCE CLOSURE PROBLEM: AN OVERVIEW, Ecol Appl,
866 18, 1351–1367, <https://doi.org/10.1890/06-0922.1>, 2008.
- 867 Foley, J. A., Prentice, I. C., Ramankutty, N., Levis, S., Pollard, D., Sitch, S., and Haxeltine, A.:
868 An integrated biosphere model of land surface processes, terrestrial carbon balance, and
869 vegetation dynamics, Global Biogeochem Cy, 10, 603–628, <https://doi.org/10.1029/96gb02692>,
870 1996.
- 871 Fowler, D., Lessard, J.-P., and Sanders, N. J.: Niche filtering rather than partitioning shapes the
872 structure of temperate forest ant communities., J Animal Ecol, 83, 943–52,
873 <https://doi.org/10.1111/1365-2656.12188>, 2013.
- 874 Friedman, J. H.: Greedy function approximation: A gradient boosting machine., Ann Statistics,
875 29, <https://doi.org/10.1214/aos/1013203451>, 2001.
- 876 Fyllas, N. M., Gloor, E., Mercado, L. M., Sitch, S., Quesada, C. A., Domingues, T. F., Galbraith,
877 D. R., Torre-Lezama, A., Vilanova, E., Ramírez-Angulo, H., Higuchi, N., et al.: Analysing
878 Amazonian forest productivity using a new individual and trait-based model (TFS v.1),
879 Geoscientific Model Development, 7, 1251–1269, <https://doi.org/10.5194/gmd-7-1251-2014>,
880 2014.
- 881 Gatti, L. V., Basso, L. S., Miller, J. B., Gloor, M., Domingues, L. G., Cassol, H. L. G., Tejada,
882 G., Aragão, L. E. O. C., Nobre, C., Peters, W., Marani, L., et al.: Amazonia as a carbon source
883 linked to deforestation and climate change, Nature, 595, 388–393,
884 <https://doi.org/10.1038/s41586-021-03629-6>, 2021.
- 885 Golaz, J., Caldwell, P. M., Roedel, L. P. V., Petersen, M. R., Tang, Q., Wolfe, J. D., Abeshu, G.,
886 Anantharaj, V., Asay-Davis, X. S., Bader, D. C., Baldwin, S. A., Bisht, G., Bogenschutz, P. A.,
887 Branstetter, M., Brunke, M. A., Brus, S. R., Burrows, S. M., et al.: The DOE E3SM Coupled
888 Model Version 1: Overview and Evaluation at Standard Resolution, J Adv Model Earth Sy, 11,
889 2089–2129, <https://doi.org/10.1029/2018ms001603>, 2019.
- 890 Hanbury-Brown, A. R., Ward, R. E., and Kueppers, L. M.: Forest regeneration within Earth
891 system models: current process representations and ways forward, New Phytol, 235, 20–40,
892 <https://doi.org/10.1111/nph.18131>, 2022.



- 893 Haverd, V., Smith, B., Cook, G. D., Briggs, P. R., Nieradzik, L., Roxburgh, S. H., Liedloff, A.,
894 Meyer, C. P., and Canadell, J. G.: A stand-alone tree demography and landscape structure
895 module for Earth system models, *Geophys Res Lett*, 40, 5234–5239,
896 <https://doi.org/10.1002/grl.50972>, 2013.
- 897 He, X., Liu, S., Xu, T., Yu, K., Gentine, P., Zhang, Z., Xu, Z., Jiao, D., and Wu, D.: Improving
898 predictions of evapotranspiration by integrating multi-source observations and land surface
899 model, *Agr Water Manage*, 272, 107827, <https://doi.org/10.1016/j.agwat.2022.107827>, 2022.
- 900 Holm, J. A., Knox, R. G., Zhu, Q., Fisher, R. A., Koven, C. D., Lima, A. J. N., Riley, W. J.,
901 Longo, M., Negrón-Juárez, R. I., Araujo, A. C., Kueppers, L. M., Moorcroft, P. R., Higuchi, N.,
902 and Chambers, J. Q.: The Central Amazon Biomass Sink Under Current and Future Atmospheric
903 CO₂: Predictions From Big-Leaf and Demographic Vegetation Models, *J Geophys Res*
904 *Biogeosciences*, 125, <https://doi.org/10.1029/2019jg005500>, 2020.
- 905 Huang, M., Xu, Y., Longo, M., Keller, M., Knox, R. G., Koven, C. D., and Fisher, R. A.:
906 Assessing impacts of selective logging on water, energy, and carbon budgets and ecosystem
907 dynamics in Amazon forests using the Functionally Assembled Terrestrial Ecosystem Simulator,
908 *Biogeosciences*, 17, 4999–5023, <https://doi.org/10.5194/bg-17-4999-2020>, 2020.
- 909 Hubau, W., Lewis, S. L., Phillips, O. L., Affum-Baffoe, K., Beeckman, H., Cuní-Sánchez, A.,
910 Daniels, A. K., Ewango, C. E. N., Fauset, S., Mukinzi, J. M., SHEIL, D., Sonké, B., Sullivan, M.
911 J. P., Sunderland, T. C. H., Taedoumg, H., Thomas, S. C., White, L. J. T., et al.: Asynchronous
912 carbon sink saturation in African and Amazonian tropical forests, *Nature*, 579, 80–87,
913 <https://doi.org/10.1038/s41586-020-2035-0>, 2020.
- 914 Hurr, G. C., Moorcroft, P. R., And, S. W. P., and Levin, S. A.: Terrestrial models and global
915 change: challenges for the future, *Global Change Biol*, 4, 581–590,
916 <https://doi.org/10.1046/j.1365-2486.1998.t01-1-00203.x>, 1998.
- 917 Jonard, M., André, F., Coligny, F. de, Wergifosse, L. de, Beudez, N., Davi, H., Ligot, G.,
918 Ponette, Q., and Vincke, C.: HETEROFOR 1.0: a spatially explicit model for exploring the
919 response of structurally complex forests to uncertain future conditions – Part 1: Carbon fluxes
920 and tree dimensional growth, *Geosci Model Dev*, 13, 905–935, <https://doi.org/10.5194/gmd-13-905-2020>, 2020.
- 922 Jung, M., Koirala, S., Weber, U., Ichii, K., Gans, F., Camps-Valls, G., Papale, D., Schwalm, C.,
923 Tramontana, G., and Reichstein, M.: The FLUXCOM ensemble of global land-atmosphere
924 energy fluxes., *Sci Data*, 6, 74, <https://doi.org/10.1038/s41597-019-0076-8>, 2019.
- 925 Kattge, J., Bönsch, G., Díaz, S., Lavorel, S., Prentice, I. C., Leadley, P., Tautenhahn, S., Werner,
926 G. D. A., Aakala, T., Abedi, M., Acosta, A. T. R., Adamidis, G. C., Adamson, K., Aiba, M.,
927 Albert, C. H., Alcántara, J. M., C. C. A., Aleixo, I., Ali, H., Amiaud, B., et al.: TRY plant trait
928 database – enhanced coverage and open access, *Global Change Biology*, 26, 119–188,
929 <https://doi.org/10.1111/gcb.14904>, 2020.



- 930 Koven, C. D., Knox, R. G., Fisher, R. A., Chambers, J. Q., Christoffersen, B. O., Davies, S. J.,
931 Detto, M., Dietze, M. C., Faybishenko, B., et al.: Benchmarking and parameter sensitivity of
932 physiological and vegetation dynamics using the Functionally Assembled Terrestrial Ecosystem
933 Simulator (FATES) at Barro Colorado Island, Panama, *Biogeosciences*, 17, 3017–3044,
934 <https://doi.org/10.5194/bg-17-3017-2020>, 2020.
- 935 Kraft, N. J. B., Valencia, R., and Ackerly, D. D.: Functional Traits and Niche-Based Tree
936 Community Assembly in an Amazonian Forest, *Science*, 322, 580–582,
937 <https://doi.org/10.1126/science.1160662>, 2008.
- 938 Kraft, N. J. B., Adler, P. B., Godoy, O., James, E. C., Fuller, S., and Levine, J. M.: Community
939 assembly, coexistence and the environmental filtering metaphor, *Funct Ecol*, 29, 592–599,
940 <https://doi.org/10.1111/1365-2435.12345>, 2015.
- 941 Lawrence, D. M., Fisher, R. A., Koven, C. D., Oleson, K. W., Swenson, S. C., Bonan, G.,
942 Collier, N., Ghimire, B., Kampenhout, L., et al.: Description of New Features, Benchmarking,
943 and Impact of Forcing Uncertainty, *J Adv Model Earth Sy*, 11, 4245–4287,
944 <https://doi.org/10.1029/2018ms001583>, 2019.
- 945 Leung, L. R., Bader, D. C., Taylor, M. A., and McCoy, R. B.: An Introduction to the E3SM
946 Special Collection: Goals, Science Drivers, Development, and Analysis, *J Adv Model Earth Sy*,
947 12, <https://doi.org/10.1029/2019ms001821>, 2020.
- 948 Li, L., Yang, Z., Matheny, A. M., Zheng, H., Swenson, S. C., Lawrence, D. M., Barlage, M.,
949 Yan, B., McDowell, N. G., and Leung, L. R.: Representation of Plant Hydraulics in the Noah-
950 MP Land Surface Model: Model Development and Multiscale Evaluation, *J Adv Model Earth*
951 *Sy*, 13, <https://doi.org/10.1029/2020ms002214>, 2021.
- 952 Liu, S. and Ng, G.-H. C.: A data-conditioned stochastic parameterization of temporal plant trait
953 variability in an ecohydrological model and the potential for plasticity, *Agr Forest Meteorol*, 274,
954 184–194, <https://doi.org/10.1016/j.agrformet.2019.05.005>, 2019.
- 955 Longo, M., Knox, R. G., Medvigy, D. M., Levine, N. M., Dietze, M. C., Kim, Y., Swann, A. L.
956 S., Zhang, K., Rollinson, C. R., Bras, R. L., Wofsy, S. C., and Moorcroft, P. R.: The biophysics,
957 ecology, and biogeochemistry of functionally diverse, vertically and horizontally heterogeneous
958 ecosystems: the Ecosystem Demography model, version 2.2 – Part 1: Model description, *Geosci*
959 *Model Dev*, 12, 4309–4346, <https://doi.org/10.5194/gmd-12-4309-2019>, 2019.
- 960 Longo, M., Saatchi, S., Keller, M., Bowman, K., Ferraz, A., Moorcroft, P. R., Morton, D. C.,
961 Bonal, D., Brando, P., Burban, B., Derroire, G., dos-Santos, M. N., Meyer, V., Saleska, S.,
962 Trumbore, S., and Vincent, G.: Impacts of Degradation on Water, Energy, and Carbon Cycling
963 of the Amazon Tropical Forests, *J Geophys Res Biogeosciences*, 125, e2020JG005677,
964 <https://doi.org/10.1029/2020jg005677>, 2020.



- 965 Lu, X., Wang, Y., Wright, I. J., Reich, P. B., Shi, Z., and Dai, Y.: Incorporation of plant traits in
966 a land surface model helps explain the global biogeographical distribution of major forest
967 functional types, *Global Ecol Biogeogr*, 26, 304–317, <https://doi.org/10.1111/geb.12535>, 2017.
- 968 Lundberg, S. and Lee, S.-I.: A Unified Approach to Interpreting Model Predictions, Arxiv, 2017.
- 969 Lundberg, S. M., Nair, B., Vavilala, M. S., Horibe, M., Eisses, M. J., Adams, T., Liston, D. E.,
970 Low, D. K.-W., Newman, S.-F., Kim, J., and Lee, S.-I.: Explainable machine-learning
971 predictions for the prevention of hypoxaemia during surgery, *Nat Biomed Eng*, 2, 749–760,
972 <https://doi.org/10.1038/s41551-018-0304-0>, 2018.
- 973 Lundberg, S. M., Erion, G., Chen, H., DeGrave, A., Prutkin, J. M., Nair, B., Katz, R.,
974 Himmelfarb, J., Bansal, N., and Lee, S.-I.: From local explanations to global understanding with
975 explainable AI for trees, *Nat Mach Intell*, 2, 56–67, <https://doi.org/10.1038/s42256-019-0138-9>,
976 2020.
- 977 Ma, L., Hurtt, G., Ott, L., Sahajpal, R., Fisk, J., Lamb, R., Tang, H., Flanagan, S., Chini, L.,
978 Chatterjee, A., and Sullivan, J.: Global Evaluation of the Ecosystem Demography Model (ED
979 v3.0), *Geoscientific Model Dev Discuss*, 2021, 1–41, <https://doi.org/10.5194/gmd-2021-292>,
980 2021.
- 981 Maréchaux, I. and Chave, J.: An individual-based forest model to jointly simulate carbon and
982 tree diversity in Amazonia: description and applications, *Ecol Monogr*, 87, 632–664,
983 <https://doi.org/10.1002/ecm.1271>, 2017.
- 984 Mason, N. W. H., Richardson, S. J., Peltzer, D. A., Bello, F. de, Wardle, D. A., and Allen, R. B.:
985 Changes in coexistence mechanisms along a long-term soil chronosequence revealed by
986 functional trait diversity: Functional diversity along ecological gradients, *J Ecol*, 100, 678–689,
987 <https://doi.org/10.1111/j.1365-2745.2012.01965.x>, 2012.
- 988 McDowell, N. G., Allen, C. D., Anderson-Teixeira, K., Aukema, B. H., Bond-Lamberty, B.,
989 Chini, L., Clark, J. S., Dietze, M., et al.: Pervasive shifts in forest dynamics in a changing world,
990 *Science*, 368, <https://doi.org/10.1126/science.aaz9463>, 2020.
- 991 McDowell, N. G., Sapes, G., Pivovarov, A., Adams, H. D., Allen, C. D., Anderegg, W. R. L.,
992 Arend, M., Breshears, D. D., Brodribb, T., et al.: Mechanisms of woody-plant mortality under
993 rising drought, CO₂ and vapour pressure deficit, *Nat Rev Earth Environ*, 3, 294–308,
994 <https://doi.org/10.1038/s43017-022-00272-1>, 2022.
- 995 McMahan, S. M., Harrison, S. P., Armbruster, W. S., Bartlein, P. J., Beale, C. M., Edwards, M.
996 E., Kattge, J., Midgley, G., Morin, X., and Prentice, I. C.: Improving assessment and modelling
997 of climate change impacts on global terrestrial biodiversity, *Trends Ecol Evol*, 26, 249–259,
998 <https://doi.org/10.1016/j.tree.2011.02.012>, 2011.
- 999 Medvigy, D., Wofsy, S. C., Munger, J. W., Hollinger, D. Y., and Moorcroft, P. R.: Mechanistic
1000 scaling of ecosystem function and dynamics in space and time: Ecosystem Demography model



- 1001 version 2, *J Geophys Res Biogeosciences* 2005 2012, 114,
1002 <https://doi.org/10.1029/2008jg000812>, 2009.
- 1003 Meng, T.-T., Wang, H., Harrison, S. P., Prentice, I. C., Ni, J., and Wang, G.: Responses of leaf
1004 traits to climatic gradients: adaptive variation versus compositional shifts, *Biogeosciences*, 12,
1005 5339–5352, <https://doi.org/10.5194/bg-12-5339-2015>, 2015.
- 1006 MICHALKO, R. and PEKÁR, S.: Niche partitioning and niche filtering jointly mediate the
1007 coexistence of three closely related spider species (Araneae, Philodromidae), *Ecol Entomol*, 40,
1008 22–33, <https://doi.org/10.1111/een.12149>, 2015.
- 1009 Mitchard, E. T. A.: The tropical forest carbon cycle and climate change, *Nature*, 559, 527–534,
1010 <https://doi.org/10.1038/s41586-018-0300-2>, 2018.
- 1011 Moorcroft, P. R.: Recent advances in ecosystem-atmosphere interactions: an ecological
1012 perspective, *Proc Royal Soc Lond Ser B Biological Sci*, 270, 1215–1227,
1013 <https://doi.org/10.1098/rspb.2002.2251>, 2003.
- 1014 Moorcroft, P. R., Hurtt, G. C., and Pacala, S. W.: A Method for Scaling Vegetation Dynamics:
1015 The Ecosystem Demography Model (ED), *Ecol Monogr*, 71, 557,
1016 <https://doi.org/10.2307/3100036>, 2001.
- 1017 Mora, C., Tittensor, D. P., Adl, S., Simpson, A. G. B., and Worm, B.: How Many Species Are
1018 There on Earth and in the Ocean?, *Plos Biol*, 9, e1001127,
1019 <https://doi.org/10.1371/journal.pbio.1001127>, 2011.
- 1020 Nearing, G. S., Kratzert, F., Sampson, A. K., Pelissier, C. S., Klotz, D., Frame, J. M., Prieto, C.,
1021 and Gupta, H. V.: What Role Does Hydrological Science Play in the Age of Machine Learning?,
1022 *Water Resour Res*, 57, <https://doi.org/10.1029/2020wr028091>, 2021.
- 1023 Nicotra, A. B., Atkin, O. K., Bonser, S. P., Davidson, A. M., Finnegan, E. J., Mathesius, U.,
1024 Poot, P., Purugganan, M. D., Richards, C. L., Valladares, F., and Kleunen, M. van: Plant
1025 phenotypic plasticity in a changing climate, *Trends Plant Sci*, 15, 684–692,
1026 <https://doi.org/10.1016/j.tplants.2010.09.008>, 2010.
- 1027 Oliveira, R. S., Eller, C. B., Barros, F. de V., Hirota, M., Brum, M., and Bittencourt, P.: Linking
1028 plant hydraulics and the fast–slow continuum to understand resilience to drought in tropical
1029 ecosystems, *New Phytol*, 230, 904–923, <https://doi.org/10.1111/nph.17266>, 2021.
- 1030 Padarian, J., McBratney, A. B., and Minasny, B.: Game theory interpretation of digital soil
1031 mapping convolutional neural networks, *Soil*, 6, 389–397, <https://doi.org/10.5194/soil-6-389-2020>, 2020.
- 1033 Pal, A., Mahajan, S., and Norman, M. R.: Using Deep Neural Networks as Cost-Effective
1034 Surrogate Models for Super-Parameterized E3SM Radiative Transfer, *Geophys Res Lett*, 46,
1035 6069–6079, <https://doi.org/10.1029/2018gl081646>, 2019.



- 1036 Piao, S., Wang, X., Wang, K., Li, X., Bastos, A., Canadell, J. G., Ciais, P., Friedlingstein, P., and
1037 Sitch, S.: Interannual variation of terrestrial carbon cycle: Issues and perspectives, *Global*
1038 *Change Biology*, 26, 300–318, <https://doi.org/10.1111/gcb.14884>, 2020.
- 1039 Poorter, L., Bongers, F., Sterck, F. J., and Wöll, H.: ARCHITECTURE OF 53 RAIN FOREST
1040 TREE SPECIES DIFFERING IN ADULT STATURE AND SHADE TOLERANCE, *Ecology*,
1041 84, 602–608, [https://doi.org/10.1890/0012-9658\(2003\)084\[0602:aorfts\]2.0.co;2](https://doi.org/10.1890/0012-9658(2003)084[0602:aorfts]2.0.co;2), 2003.
- 1042 Prentice, I. C., Webb, R. S., Ter-Mikhaelian, M. T., Solomon, A. M., Smith, T. M., Pitovranov,
1043 S. E., Nikolov, N. T., Minin, A. A., Leemans, R., et al.: Developing a global vegetation
1044 dynamics model: Results of an IIASA summer workshop, Research Report RR-89-7,
1045 International Institute for Applied Systems Analysis, Laxenburg, Austria, available at:
1046 <http://pure.iiasa.ac.at/3223>, 1989.
- 1047 Purves, D. W., Lichstein, J. W., Strigul, N., and Pacala, S. W.: Predicting and understanding
1048 forest dynamics using a simple tractable model, *Proc National Acad Sci*, 105, 17018–17022,
1049 <https://doi.org/10.1073/pnas.0807754105>, 2008.
- 1050 Restrepo-Coupe, Rocha, N., H.R., Hutya, L.R., et al.: LBA-ECO CD-32 Flux Tower Network
1051 Data Compilation, Brazilian Amazon: 1999-2006, V2. ORNL DAAC,
1052 <https://doi.org/10.3334/ORNLDAAC/1842>, 2021.
- 1053 Reich, P. B.: The world-wide ‘fast–slow’ plant economics spectrum: a traits manifesto, *J Ecol*,
1054 102, 275–301, <https://doi.org/10.1111/1365-2745.12211>, 2014.
- 1055 Rocha H. R., Manzi A. O., Shuttleworth J.: Evapotranspiration, Amazonia and Global Change, ,
1056 *Geophysical Monograph Series Volume 186*, 261–272, <https://doi.org/10.1029/2008GM000817>,
1057 2009.
- 1058 Rouholahnejad, E., Abbaspour, K. C., Vejdani, M., Srinivasan, R., Schulin, R., and Lehmann,
1059 A.: A parallelization framework for calibration of hydrological models, *Environ Modell Softw*,
1060 31, 28–36, <https://doi.org/10.1016/j.envsoft.2011.12.001>, 2012.
- 1061 Rüger, N., Condit, R., Dent, D. H., DeWalt, S. J., Hubbell, S. P., Lichstein, J. W., Lopez, O. R.,
1062 Wirth, C., and Farris, C. E.: Demographic trade-offs predict tropical forest dynamics, *Science*,
1063 368, 165–168, <https://doi.org/10.1126/science.aaz4797>, 2020.
- 1064 Sakschewski, B., Bloh, W., Boit, A., Rammig, A., Kattge, J., Poorter, L., Peñuelas, J., and
1065 Thonicke, K.: Leaf and stem economics spectra drive diversity of functional plant traits in a
1066 dynamic global vegetation model, *Global Change Biol*, 21, 2711–2725,
1067 <https://doi.org/10.1111/gcb.12870>, 2015.
- 1068 Sakschewski, B., Bloh, W. von, Boit, A., Poorter, L., Peña-Claros, M., Heinke, J., Joshi, J., and
1069 Thonicke, K.: Resilience of Amazon forests emerges from plant trait diversity, *Nature Climate*
1070 *Change*, 6, 1032–1036, <https://doi.org/10.1038/nclimate3109>, 2016.



- 1071 Sato, H., Itoh, A., and Kohyama, T.: SEIB–DGVM: A new Dynamic Global Vegetation Model
1072 using a spatially explicit individual-based approach, *Ecol Model*, 200, 279–307,
1073 <https://doi.org/10.1016/j.ecolmodel.2006.09.006>, 2007.
- 1074 Sawada, Y.: Machine Learning Accelerates Parameter Optimization and Uncertainty Assessment
1075 of a Land Surface Model, *J Geophys Res Atmospheres*, 125,
1076 <https://doi.org/10.1029/2020jd032688>, 2020.
- 1077 Shen, C.: A Transdisciplinary Review of Deep Learning Research and Its Relevance for Water
1078 Resources Scientists, *Water Resour Res*, 54, 8558–8593, <https://doi.org/10.1029/2018wr022643>,
1079 2018.
- 1080 Siefert, A., Violle, C., Chalmandrier, L., Albert, C. H., et al.: A global meta-analysis of the
1081 relative extent of intraspecific trait variation in plant communities, *Ecol Lett*, 18, 1406–1419,
1082 <https://doi.org/10.1111/ele.12508>, 2015.
- 1083 Sit, M., Demiray, B. Z., Xiang, Z., Ewing, G. J., Sermet, Y., and Demir, I.: A comprehensive
1084 review of deep learning applications in hydrology and water resources, *Water Sci Technol*, 82,
1085 2635–2670, <https://doi.org/10.2166/wst.2020.369>, 2020.
- 1086 Sitch, S., Smith, B., Prentice, I. C., Arneth, A., Bondeau, A., Cramer, W., Kaplan, J. O., Levis,
1087 S., Lucht, W., Sykes, M. T., Thonicke, K., and Venevsky, S.: Evaluation of ecosystem dynamics,
1088 plant geography and terrestrial carbon cycling in the LPJ dynamic global vegetation model: LPJ
1089 DYNAMIC GLOBAL VEGETATION MODEL, *Global Change Biol*, 9, 161–185,
1090 <https://doi.org/10.1046/j.1365-2486.2003.00569.x>, 2003.
- 1091 Snell, R. S., Huth, A., Nabel, J. E. M. S., Bocedi, G., Travis, J. M. J., Gravel, D., Bugmann, H.,
1092 Gutiérrez, A. G., Hickler, T., Higgins, S. I., Reineking, B., Scherstjanoi, M., Zurbriggen, N., and
1093 Lischke, H.: Using dynamic vegetation models to simulate plant range shifts, *Ecography*, 37,
1094 1184–1197, <https://doi.org/10.1111/ecog.00580>, 2014.
- 1095 Snoek, J., Larochelle, H., and Adams, R. P.: Practical Bayesian Optimization of Machine
1096 Learning Algorithms, *Arxiv*, 2012.
- 1097 Stark, S. C., Leitold, V., Wu, J. L., Hunter, M. O., Castilho, C. V. de, Costa, F. R. C., McMahon,
1098 S. M., Parker, G. G., Shimabukuro, M. T., et al.: Amazon forest carbon dynamics predicted by
1099 profiles of canopy leaf area and light environment, *Ecol Lett*, 15, 1406–1414,
1100 <https://doi.org/10.1111/j.1461-0248.2012.01864.x>, 2012.
- 1101 Strigul, N., Pristinski, D., Purves, D., Dushoff, J., and Pacala, S.: SCALING FROM TREES TO
1102 FORESTS: TRACTABLE MACROSCOPIC EQUATIONS FOR FOREST DYNAMICS, *Ecol*
1103 *Monogr*, 78, 523–545, <https://doi.org/10.1890/08-0082.1>, 2008.
- 1104 Swenson, N. G. and Enquist, B. J.: Opposing assembly mechanisms in a Neotropical dry forest:
1105 implications for phylogenetic and functional community ecology, *Ecology*, 90, 2161–2170,
1106 <https://doi.org/10.1890/08-1025.1>, 2009.



- 1107 Thakur, M. P. and Wright, A. J.: Environmental Filtering, Niche Construction, and Trait
1108 Variability: The Missing Discussion, *Trends Ecol Evol*, 32, 884–886,
1109 <https://doi.org/10.1016/j.tree.2017.09.014>, 2017.
- 1110 Tsai, W.-P., Feng, D., Pan, M., Beck, H., Lawson, K., Yang, Y., Liu, J., and Shen, C.: From
1111 calibration to parameter learning: Harnessing the scaling effects of big data in geoscientific
1112 modeling, *Nat Commun*, 12, 5988, <https://doi.org/10.1038/s41467-021-26107-z>, 2021.
- 1113 Uriarte, M., Swenson, N. G., Chazdon, R. L., Comita, L. S., Kress, W. J., Erickson, D., Forero-
1114 Montaña, J., Zimmerman, J. K., and Thompson, J.: Trait similarity, shared ancestry and the
1115 structure of neighbourhood interactions in a subtropical wet forest: implications for community
1116 assembly, *Ecol Lett*, 13, 1503–1514, <https://doi.org/10.1111/j.1461-0248.2010.01541.x>, 2010.
- 1117 Violle, C., Enquist, B. J., McGill, B. J., Jiang, L., Albert, C. H., Hulshof, C., Jung, V., and
1118 Messier, J.: The return of the variance: intraspecific variability in community ecology, *Trends*
1119 *Ecol Evol*, 27, 244–252, <https://doi.org/10.1016/j.tree.2011.11.014>, 2012.
- 1120 Wang, C., Duan, Q., Gong, W., Ye, A., Di, Z., and Miao, C.: An evaluation of adaptive surrogate
1121 modeling based optimization with two benchmark problems, *Environ Modell Softw*, 60, 167–
1122 179, <https://doi.org/10.1016/j.envsoft.2014.05.026>, 2014.
- 1123 Wang, S. S. -C., Qian, Y., Leung, L. R., and Zhang, Y.: Identifying Key Drivers of Wildfires in
1124 the Contiguous US Using Machine Learning and Game Theory Interpretation, *Earth's Futur*, 9,
1125 e2020EF001910, <https://doi.org/10.1029/2020ef001910>, 2021.
- 1126 Wang, S. S.-C., Qian, Y., Leung, L. R., and Zhang, Y.: Interpreting machine learning prediction
1127 of fire emissions and comparison with FireMIP process-based models, *Atmos Chem Phys*, 22,
1128 3445–3468, <https://doi.org/10.5194/acp-22-3445-2022>, 2022.
- 1129 Watson-Parris, D., Williams, A., Deaconu, L., and Stier, P.: Model calibration using ESEm
1130 v1.1.0 – an open, scalable Earth system emulator, *Geosci Model Dev*, 14, 7659–7672,
1131 <https://doi.org/10.5194/gmd-14-7659-2021>, 2021.
- 1132 Weng, E. S., Malyshev, S., Lichstein, J. W., Farris, C. E., Dybzinski, R., Zhang, T.,
1133 Shevliakova, E., and Pacala, S. W.: Scaling from individual trees to forests in an Earth system
1134 modeling framework using a mathematically tractable model of height-structured competition,
1135 *Biogeosciences*, 12, 2655–2694, <https://doi.org/10.5194/bg-12-2655-2015>, 2015.
- 1136 Wilson, K., Goldstein, A., Falge, E., Aubinet, M., Baldocchi, D., Berbigier, P., Bernhofer, C.,
1137 Ceulemans, R., Dolman, H., Field, C., et al.: Energy balance closure at FLUXNET sites, *Agr*
1138 *Forest Meteorol*, 113, 223–243, [https://doi.org/10.1016/s0168-1923\(02\)00109-0](https://doi.org/10.1016/s0168-1923(02)00109-0), 2002.
- 1139 Wright, I. J., Reich, P. B., Cornelissen, J. H. C., Falster, D. S., Garnier, E., Hikosaka, K.,
1140 Lamont, B. B., Lee, W., Oleksyn, J., Osada, N., Poorter, H., Villar, R., Warton, D. I., and
1141 Westoby, M.: Assessing the generality of global leaf trait relationships, *New Phytol*, 166, 485–
1142 496, <https://doi.org/10.1111/j.1469-8137.2005.01349.x>, 2005.



- 1143 Xu, T. and Liang, F.: Machine learning for hydrologic sciences: An introductory overview,
1144 Wiley Interdiscip Rev Water, 8, <https://doi.org/10.1002/wat2.1533>, 2021.
- 1145 Zhang, J., Bras, R. L., Longo, M., and Scalley, T. H.: The impact of hurricane disturbances on a
1146 tropical forest: implementing a palm plant functional type and hurricane disturbance module in
1147 ED2-HuDi V1.0, Geosci Model Dev, 15, 5107–5126, [https://doi.org/10.5194/gmd-15-5107-](https://doi.org/10.5194/gmd-15-5107-2022)
1148 [2022](https://doi.org/10.5194/gmd-15-5107-2022), 2022.
- 1149 Zheng, Z., Curtis, J. H., Yao, Y., Gasparik, J. T., Anantharaj, V. G., Zhao, L., West, M., and
1150 Riemer, N.: Estimating Submicron Aerosol Mixing State at the Global Scale With Machine
1151 Learning and Earth System Modeling, Earth Space Sci, 8, <https://doi.org/10.1029/2020ea001500>,
1152 2021a.
- 1153 Zheng, Z., Zhao, L., and Oleson, K. W.: Large model structural uncertainty in global projections
1154 of urban heat waves, Nat Commun, 12, 3736, <https://doi.org/10.1038/s41467-021-24113-9>,
1155 2021b.
- 1156 Zheng, Z., West, M., Zhao, L., Ma, P.-L., Liu, X., and Riemer, N.: Quantifying the structural
1157 uncertainty of the aerosol mixing state representation in a modal model, Atmos Chem Phys, 21,
1158 17727–17741, <https://doi.org/10.5194/acp-21-17727-2021>, 2021c.
- 1159 Zhu, Q., Li, F., Riley, W. J., Xu, L., Zhao, L., Yuan, K., Wu, H., Gong, J., and Randerson, J.:
1160 Building a machine learning surrogate model for wildfire activities within a global Earth system
1161 model, Geosci Model Dev, 15, 1899–1911, <https://doi.org/10.5194/gmd-15-1899-2022>, 2022.
- 1162 Zuleta, D., Duque, A., Cardenas, D., Muller-Landau, H. C., and Davies, S. J.: Drought-induced
1163 mortality patterns and rapid biomass recovery in a terra firme forest in the Colombian Amazon,
1164 Ecology, 98, 2538–2546, <https://doi.org/10.1002/ecy.1950>, 2017.